TITLE

The formin DAAM is required for coordination of the actin and microtubule cytoskeleton in axonal growth cones

RUNNING TITLE: Axonal actin/MT coordination

Szilárd Szikora[1], István Földi[1], Krisztina Tóth[1], Ede Migh[1], Andrea Vig[2], Beáta Bugyi[2,3], József Maléth[4], Péter Hegyi[4,5], Péter Kaltenecker[6], Natalia Sanchez-Soriano[6] and József Mihály[1*]

[1] Institute of Genetics, Biological Research Centre, Hungarian Academy of Sciences, MTA-SZBK NAP B Axon Growth and Regeneration Group, Temesvári krt. 62, Szeged, H-6726, Hungary

[2] University of Pécs, Medical School, Department of Biophysics, Szigeti str. 12, Pécs, H-7624, Hungary

[3] Szentágothai Research Center, Ifjúság str. 34, Pécs, H-7624, Hungary

[4] MTA-SZTE Translational Gastroenterology Research Group, Szeged, Hungary

[5] Institute for Translational Medicine, University of Pecs

[6] Institute for Translational Medicine, Department of Cellular and Molecular Physiology, University of Liverpool

* Author for correspondence (mihaly.jozsef@brc.mta.hu)

KEY WORDS: actin, microtubule, formin, DAAM, growth cone, Drosophila

SUMMARY STATEMENT

We provide novel insights into the mechanisms of actin-microtubule crosstalk in axonal growth cones by describing the role of a formin protein in *Drosophila* neurons.

ABSTRACT

Directed axonal growth depends on proper coordination of the actin and microtubule cytoskeleton in the growth cone. However, despite the relatively large number of proteins implicated in actin-microtubule cross-talk, the mechanisms whereby actin polymerization is coupled to microtubule stabilization and advancement in the peripheral growth cone remained largely unclear. Here we identified the formin DAAM as a novel factor playing a role in concerted regulation of actin and microtubule remodeling in *Drosophila* primary neurons. *In vitro* DAAM binds to F-actin as well as microtubules and it has the ability to crosslink the two filament systems. Accordingly, DAAM associates with the neuronal cytoskeleton, and a significant fraction of DAAM accumulates at places where the actin filaments overlap with that of microtubules. Loss of *DAAM* affects growth cone and microtubule morphology and several aspects of microtubule dynamics, whereas biochemical and cellular assays revealed a microtubule stabilization activity and binding to the microtubule tip protein EB1. Together these data suggest that besides operating as an actin assembly factor, DAAM is involved in linking filopodial actin remodeling to microtubule stabilization during axonal growth.

INTRODUCTION

Directional movement of axons, governed by their distally located growth cones, is elicited by coordinated changes of peripheral F-actin (filamentous-actin) and central microtubule networks (Dent and Gertler, 2003; Lowery and Van Vactor, 2009). F-actin in growth cone periphery is localized to two main structures, filopodia and lamellipodia. Splayed microtubules emanating from the central axonal microtubule bundles dynamically invade and scan the F-actin rich periphery, often reaching deep into filopodia (Dent and Gertler, 2003; Lowery and Van Vactor, 2009). Filopodial F-actin bundles can act as guides for these dynamic microtubules, and it is thought that this actin-microtubule crosstalk followed by microtubule and filopodia stabilization is a key step of growth cone advance. Most proteins that have so far been linked to the molecular mechanisms of the interaction of actin and microtubules belong to the microtubule plus-end tracking proteins (+TIPs), such as CLASP, CLIP-170, APC, EB1/3, LIS1 and Spectraplakin/ACF7 (recently reviewed in (Bearce et al., 2015; Cammarata et al., 2016; Coles and Bradke, 2015). Although the role of these proteins in growth cone guidance is supported by genetic, biochemical and advanced microscopic assays, these large proteins operate in complex interaction networks posing a great challenge for dissecting how they precisely function.

Beyond the classical +TIPs, the number of proteins that may couple microtubules to F-actin dynamics at plus-ends is still expanding (Coles and Bradke, 2015; Jiang et al., 2012). For example, recent work identified members of the formin family as regulators of actin and microtubule crosstalk in non-neuronal cells (Bartolini et al., 2008; Chesarone et al., 2010; Gaillard et al., 2011; Rosales-Nieves et al., 2006; Young and Copeland, 2010). Formins are well characterized actin assembly factors that promote the formation of unbranched actin cables by facilitating their nucleation and elongation (Chesarone et al., 2010; Schonichen and Geyer, 2010). These multidomain proteins contain two highly conserved signature domains, the FH1 and FH2 formin homology domains. The dimeric FH2 nucleates actin filaments and supports elongation by remaining processively attached to their barbed ends (Higashida et al., 2004; Kovar and Pollard, 2004; Watanabe and Higashida, 2004), whereas the proline-rich FH1 domain accelerates elongation by recruiting profilin-bound actin monomers (Li and Higgs, 2003; Sagot et al., 2002). Some formins contain several other conserved regions including the N-terminally located GBD (GTPase binding domain), DID (diaphanous inhibitory domain), DD (dimerization domain), CC (coiled-coil region) and the C-terminal DAD (diaphanous auto-regulatory domain) (Alberts, 2001; Chesarone et al., 2010; Li and

Higgs, 2003; Otomo et al., 2005; Rose et al., 2005). These domains are involved in the spatial and temporal regulation of the actin assembly activity provided by the FH2 domain (Chesarone et al., 2010). In addition, it has also been shown that a number of formins influence microtubule (MT) stability and organization (Bartolini and Gundersen, 2010). Consistently, many formins are able to bind to MTs *in vitro* through their actin binding FH2 domain and in some cases with their C-terminal region (Bartolini et al., 2008; Chesarone et al., 2010; Gaillard et al., 2011; Roth-Johnson et al., 2014; Young et al., 2008; Zhou et al., 2006). The presence of both an actin- and a microtubule-binding domain might allow these proteins to crosslink the cytoskeletal components directly, such as Cappuccino does *in vitro* and presumably in *Drosophila* oocytes (Rosales-Nieves et al., 2006). Conversely, instead of or in parallel to direct binding, the Diaphanous-related formins (DRFs) mDia1, mDia2 and mDia3 appear to stabilize MTs in fibroblast cells by +TIP binding through EB1, CLIP-170 or APC (Cheng et al., 2011; Lewkowicz et al., 2008; Wen et al., 2004). Interestingly, mDia2 is able to stabilize MTs and bind to +TIPs independently of its actin nucleation activity (Bartolini et al., 2008). Finally, recent work revealed that CLIP-170 binds tightly to mDia1 to increase the rate of actin polymerization from MT plus-ends (Henty-Ridilla et al., 2016). Despite these advances, the *in vivo* contribution of formins to MT and F-actin interactions in axonal growth cones remained elusive.

In this paper, we report the characterization of the role of the formin family protein DAAM (Dishevelled associated activator of morphogenesis) in concerted regulation of actin and MT remodeling in axons of *Drosophila* neurons. We show that *Drosophila* DAAM partially colocalizes with both major cytoskeletal systems in neurons, and it is able to crosslink actin filaments with MTs *in vitro*. DAAM stabilizes MTs against cold- or **nocodazole**-induced depolymerization, and the absence of *DAAM* impairs neuronal MT organization and dynamics. Although DAAM has the ability to bind MTs directly, it also binds to an MT plus-end tracking protein, EB1, and often localizes to MT plus tips. This suggests that, similar to migrating cells, a formin/+TIP dependent mechanism is crucial to govern actin/MT coordination in growing axons.

RESULTS

DAAM localizes to axonal microtubule bundles and physically interacts with microtubules

Previously we have shown that DAAM plays an essential role in differentiation of the embryonic nervous system (Matusek et al., 2008) and the adult brain (Gombos et al., 2015). *In vitro* and *in vivo* studies revealed that DAAM behaves as a *bona fide* formin and it is required for filopodia formation (Barko et al., 2010; Matusek et al., 2008), similarly to its vertebrate orthologue, Daam1 (Jaiswal et al., 2013a). Furthermore, the observed cellular phenotypes, i.e. the reduced filopodia number and length coincide with DAAM accumulation along the shaft and on the tip of filopodia (Goncalves-Pimentel et al., 2011; Jaiswal et al., 2013a; Matusek et al., 2008). Although formins are primarily considered as actin assembly machineries, numerous studies demonstrated that some formins are able to interact with MTs either directly or indirectly (Bartolini and Gundersen, 2010; Bartolini et al., 2008; Dahlgaard et al., 2007; Gaillard et al., 2011; Gasteier et al., 2005; Rosales-Nieves et al., 2006; Roth-Johnson et al., 2014; Shaye and Greenwald, 2015). Since the highly conserved FH2 was identified as the main MT interacting domain in DRFs, it is reasonable to assume that DAAM might also be able to interact with MTs. Therefore, to further elaborate on the functions of DAAM, we reassessed its sub-cellular localization by performing immunostaining of endogenous DAAM in cultured primary neurons. We found that, although DAAM primarily localizes to F-actin rich structures, i.e. the filopodia, lamellipodia and cortical actin (Fig. S1 A-D, I, I'; Movie 1), a significant fraction of DAAM accumulated **in punctae** along the axonal MTs (Fig. 1A-D, Fig. S1 E-H). To estimate the sub-cellular distribution of DAAM, we quantified the protein-protein proximity index (PPI) (Wu et al., 2010; Zinchuk et al., 2011) between DAAM and actin, and DAAM and tubulin, respectively. The analysis revealed that ~47% (PPI: 0.47±0.05) of DAAM is associated with the actin cytoskeleton. Surprisingly however, another ~37% (PPI: 0.37±0.05) exhibited an overlap with MTs (Fig. 1E). Most notably, we detected frequent DAAM accumulation on axonal MT ends (36±14 %) (Fig. 1F). These observations were further verified with a second, independently created DAAM antibody (Fig. S3 G), leading to very similar results (Fig. S1 E-H). Thus, besides actin, DAAM is often localized to MTs in axonal growth cones pointing towards MT related functions.

To begin to address whether DAAM interacts with MTs, GST-tagged DAAM fragments were purified and subsequently used in an MT co-sedimentation and a GST pull-down assay to test for direct interaction (Figs. 1G, H and S2 A-E). Both assays indicated that, unlike the purified GST protein used as negative control, a DAAM fragment comprising of the FH1 and FH2 domains was able to bind to taxol-stabilized MTs, while mutation of the conserved amino acid (I732A) playing a critical role in actin interaction, did not affect the interaction between GST::FH1FH2 and MTs. In addition to the FH2 domain, the C-terminal region of some formins was also shown to contribute to MT-binding (Gaillard et al., 2011; Roth-Johnson et al., 2014; Young et al., 2008), thus we also investigated the effect of the C-terminal region of DAAM. It appeared that the DAD domain alone did not bind to MTs, however the C-terminal tail (CT) region has an MT-binding capability. It has been shown that MT binding by the tail region of different formins is mediated by ionic interactions between the basic amino acids of the tail domain and the acidic MT surface (Gaillard et al., 2011; Roth-Johnson et al., 2014). The CT domain of DAAM is also basic with a pI of 11.6., and in line with former data, a mutant CT fragment (GST::DAD-CT^{R-A}) where the basic amino acids were changed to alanines was not able to bind to taxol-stabilized MTs.

In addition to direct MT binding, several formins were shown to associate with MTs through +TIP binding. Consistent with its MT plus end localization (Fig. 1F), DAAM was co-immunoprecipitated with EB1 (an abundant +TIP in this system) from lysates of S2 cells transfected with 3xFlag-tagged constitutively active DAAM, lacking the DAD domain (Fig. 1I). Collectively, these studies indicate that *Drosophila* DAAM, similarly to other formins, has the ability to physically interact with MTs via its FH2 as well as CT domains. Besides direct interaction, DAAM copurifies with EB1 suggesting an alternative mode of MT binding, presumably restricted to MT plus ends.

DAAM regulates the length and organization of axonal microtubule bundles

The sub-cellular localization and the *in vitro* assays suggest that DAAM might play a role in the regulation of MT organization during axon growth. Therefore, we next asked how loss of *DAAM* affects MT morphology in primary neurons. Since the maternal *DAAM* product is present in the embryos (Matusek et al., 2006), we generated primary neuronal cultures from $DAAM^{mat/zyg}$ mutant embryos (Matusek et al., 2008) in which maternal and zygotic *DAAM* functions are both impaired. Previously we demonstrated that these neurons are able to develop axons similar to the wild type control neurons, although the number and length of

growth cone filopodia are significantly decreased (Matusek et al., 2008). In the present study we measured the length of the axonal MT bundles after tubulin staining, using the semiautomatic NeuronJ plugin (Meijering et al., 2004), and revealed that axonal MT bundles, and consequently, axons are significantly (p=0.016) shorter in the *DAAM*$^{mat/zyg}$ mutant neurons (9.67±0.75µm, n=152) as compared to wild type controls (16.36±2.2µm, n=235) (Fig. 2A-B' and F). Moreover, we also studied MT morphology (Fig. 2E and G), and noted that in *DAAM*$^{mat/zyg}$ mutant neurons the frequency of looped and spread MTs is decreased, while the frequency of bundled MTs is increased significantly (p=0.0286) (Fig. 2G).

To further elaborate on the role of DAAM, we overexpressed an activated form of DAAM (CDAAM) lacking its N-terminal regions including the DID domain crucial for autoinhibition (Liu et al., 2008), by using the pan-neuronal *elav-Gal4* driver. Similar to *DAAM*$^{mat/zyg}$ mutant neurons, the axonal MT bundles were shorter (p=0.0011) in CDAAM expressing cells (14.88±0.21 µm, n=178) as compared to controls (21.51±1.15 µm, n=182) (Fig. 2C-D' and F). In contrast to *DAAM*$^{mat/zyg}$ neurons, the frequency of looped and spread MTs increased, while the frequency of bundled MTs decreased in CDAAM expressing cells (Fig. 2G). Thus, the loss- and gain-of-function studies both indicate a role in the regulation of axonal microtubule length and organization.

DAAM regulates axonal microtubule dynamics

As deviations in the organization of axonal MTs are often linked to impaired MT dynamics, we next sought to examine MT dynamics *in vivo*, in the absence of DAAM. Microtubule dynamics were quantified by using ImageJ's TrackMate plugin (Tinevez et al., 2016), following live acquisition of high-resolution images of neurons (6-9 hours in vitro, HIV) expressing EB1::GFP, a marker of MT plus ends (Morrison et al., 2002; Stepanova et al., 2003) (Figs. 3A, B and S3 H). Time lapse recordings were deconvolved and pre-filtered with a custom made difference of Gaussian filter to enhance the signal of interest and to exclude false positive hits (Fig. S3 A-B"; Movie 2). The analyses of EB1::GFP track velocity in wild type neurons revealed that MTs tend to slow down upon entering the growth cones, showing a slight, but consistent growth velocity difference between the growth cone (6.54 µm×min^{-1}) and the axonal shaft MTs (8.12 µm×min^{-1}) (Fig. 3C). For this reason, in the following studies MT dynamics in growth cones and axonal shafts were analyzed separately. Because EB1 is known to promote MT growth by preventing MT catastrophes (Komarova et al., 2009), as a further control we compared MT growth velocity in cultured neurons expressing either

EB1::GFP or Jupiter::GFP (another widely used marker of microtubule dynamics) (Karpova et al., 2006). We measured the dynamic instability parameters of individual MTs in the growth cone and found no significant differences between EB1::GFP or Jupiter::GFP (6.47±1.5, n=8) expressing neurons (Fig. S3 C-F), and hence, during our subsequent studies we used EB1::GFP to monitor MT dynamics.

First we compared microtubule growth velocities in control and *DAAM*$^{mat/zyg}$ mutant neurons. We found that the median growth velocity measured in *DAAM*$^{mat/zyg}$ mutant neurons was ~91% higher in the growth cones and ~80% higher in the axon shaft compared to the controls ($p<0.0001$ for both) (Fig. 3D; Movie 3). Parallel to that, lifetime measurements of growth cone MTs by utilizing the Kaplan-Meier estimator revealed a reduction in MT lifetime of the mutant neurons ($p<0.0001$) (Fig. 3E). The presence of DAAM seems to reduce MT growth rate and to enhance lifetime by reducing catastrophe frequency. Thus, these experiments showed that *DAAM* affects MT dynamics in neurites, which is likely to be the cause of the altered MT organization phenotypes observed previously. In line with former observations of Bartolini et al., 2008 for mDia2, it appears that increased MT dynamics is paralleled with reduced lifetime that would be consistent with a role in MT stabilization.

DAAM is involved in retrograde translocation of microtubules in growth cone filopodia

To better understand the mechanisms of how DAAM affects MT dynamics, we focused our attention to the individual pioneer microtubules, which extend into the growth cone periphery. Pioneer microtubules are of particular importance, since their entry into the filopodia and their subsequent stabilization is essential prior to growth cone turning (Buck and Zheng, 2002) and axon branching (Dent and Kalil, 2001). Expression of EB1::GFP is a suitable tool to follow the plus end of these MTs (Fig. 4A) as in most cases it is obvious when they enter filopodia, where they subsequently disappear at some point along their length, presumably because the MT has either stopped growing or depolymerized. To follow pioneer MT growth, we recorded kymographs along the axis of filopodia, then we calculated the directionality distributions of these graphs to differentiate between anterograde displacement, pause and retrograde translocation (Figs. 4B-C', E-F' and S3 H-L). We observed that the EB1::GFP signal frequently paused and/or moved rearwards in the growth cone filopodia of wild type cells (Fig. 4B, B'). Given that EB1 decorates only the polymerizing end of MTs, it suggests that these MTs underwent retrograde translocation which is a commonly observed phenomenon in the growth cone periphery (Schaefer et al., 2008). It is thought that MTs tend to couple to the retrograde actin flow through transient interactions and they are transported back as they

assemble (Marx et al., 2013) (consistently, in our primary neurons the retrograde MT translocation rate appears similar to that of retrograde actin flow, ~5.3µm*min^{-1}). Therefore, the retrograde actin flow poses a dynamic barrier to pioneer microtubules and removes them from the growth cone periphery (Schaefer et al., 2002; Schaefer et al., 2008). Remarkably, however, in *DAAM*$^{mat/zyg}$ mutant neurons we rarely observed pause or retrograde translocation of MTs in the filopodia (Fig. 4C, C'). The frequency of these events was significantly lower as compared to control cells (p=0.02) (Fig. 4D-F'). Therefore, we conclude that, at least in the pioneer MTs, the lack of DAAM reduces the retrograde translocation rate of MTs which is consistent with the increased MT growth velocity.

Direct versus indirect effects on microtubule dynamics upon loss of DAAM

Since formins were originally described as actin cytoskeleton regulators, the question arises as to whether the microtubule cytoskeleton related phenotypes are direct effects of the absence of DAAM or the consequence of the impaired actin cytoskeleton. To elucidate the role of the actin cytoskeleton on MT dynamics, we disturbed the actin cytoskeleton by latrunculin A, a drug which sequesters G-actin and promotes depolymerization (Coue et al., 1987; Yarmola et al., 2000). Primary neurons expressing Actin5C::GFP treated with 200nM latrunculin A showed signs of actin cytoskeleton breakdown in the growth cone as early as 30-60 seconds after treatment. This depolymerization plateaus after ~5 minutes when the stereotypic searching movements of filopodia completely disappear (Fig. S4 A-D; Movie 4). After establishing the F-actin breakdown protocol, we applied the same conditions to primary neurons expressing EB1::GFP, and measured MT growth dynamics in the 5-20 minute zone after treatment. We found that median growth velocity is increased both in the axon shaft and the growth cone region (Fig. 3D; Movie 5). Although this increase was similar to the one observed in *DAAM*$^{mat/zyg}$ neurons, we noted the formation of long, slender microtubule containing protrusions, which was not observed in *DAAM*$^{mat/zyg}$ neurons (Fig. S4 E-I; Movie 5). These results indicate that the F-actin network forms a barrier to MT growth in axons which was already reported in growth cones (Burnette et al., 2007; Forscher and Smith, 1988; Zhou and Cohan, 2004) but seems to apply for the shaft as well. Although the latter may imply the existence of an unexplored actin/MT crosstalk in axonal shafts, subsequently we focused our studies on the peripheral growth cone.

We reasoned that the changes in MT dynamics upon loss of DAAM might result from a slower actin retrograde flow or a change in the coupling of microtubules to the retrograde flow, or a combination of these two effects. To begin to test these alternatives, we compared

the retrograde actin flow in filopodia of wild type and *DAAM* mutant neurons. First, we followed growth-cone motility by measuring filopodial dynamics in neurons expressing Actin5C::GFP (Movie 6). Live recordings (7-9 HIV) revealed that the Actin5C::GFP signal was slightly fainter in $DAAM^{mat/zyg}$ neurons as compared to wild type neurons, and in accordance with previous findings (Matusek et al., 2008), filopodia number and length were reduced (Fig. 5B, C). To quantify the dynamic properties of growth cone filopodia, we recorded kymographs along the axis of the filopodia and calculated their extension and retraction velocity based on their tip displacement as a function of time. The mean extension velocity elevated by 28% (not significant) whereas the mean retraction rate decreased by 33% ($p=0.0096$) in the $DAAM^{mat/zyg}$ mutant neurons as compared to wild type (Fig. 5E, F). Moreover, by analyzing the fluorescent speckle pattern (Waterman-Storer and Salmon, 1998) (Fig. 5D, D') of the Actin5C::GFP signal, we determined that the mean velocities of the retrograde actin flow remained constant as the filopodia extended or retracted (Bornschlogl et al., 2013). The kymographs also revealed that the rate of the retrograde flow highly correlates with the retraction rate of the filopodia, both in wild type and $DAAM^{mat/zyg}$ neurons. Consistent with the reduced filopodia retraction rate, retrograde flow is decreased by 37.5% (not significant) in the $DAAM^{mat/zyg}$ neurons (Fig. 5G). Since the extension and retraction rates of the growth cone filopodia depend on the retrograde flow and the growth rate of the filopodial F-actin bundle, i.e. the polymerization rate of newly incorporated actin at the filopodial tip, we could calculate the plus end dynamics of the actin filaments during filopodia extension and retraction (Fig. 5A, H). We found that during filopodia extension the plus end growth of actin filaments exceeds the retrograde flow, and this rate is 20% faster (not significant) in $DAAM^{mat/zyg}$ neurons as compared to wild type (Fig. 5I). In most filopodia the plus end of the actin filament appears to be stalled during retraction both in wild type and $DAAM^{mat/zyg}$ neurons (Fig. 5J), therefore the retraction completely depends on the retrograde flow.

In summary, we revealed that although the actin depolymerizing drug, latrunculin A, had similar effects on MT growth dynamics as to the lack of *DAAM*, it also induced the formation of long, filopodia-like protrusions, never observed in *DAAM* mutant neurons, and henceforth these effects are clearly not identical. Moreover, we found that the absence of DAAM has a very weak effect on the retrograde actin flow, while the retrograde MT translocation frequency exhibits a considerable reduction in the mutant neurons. Therefore, these data suggest that the effect of DAAM on MT dynamics is unlikely to be an indirect (or largely indirect) effect due to altered actin dynamics (i.e. reduced retrograde actin flow), instead they may indicate a failure in proper coordination of actin and MT dynamics.

DAAM stabilizes microtubules *in vitro* and *in vivo*

Consistent with findings for some other members of the formin protein family (Bartolini et al., 2008; Chesarone et al., 2010; Gaillard et al., 2011), DAAM appears to promote MT stabilization in primary neurons as suggested by our MT dynamics studies. To test it more directly, we examined whether DAAM protects against MT destabilization in two different conditions. Firstly, an MT co-sedimentation assay was used to measure the effect of cold treatment on preassembled MTs in the presence or absence of purified GST::FH1FH2 protein. In accordance with our expectation, the presence of FH1FH2 was able to protect MTs against cold-induced depolymerization indicated by the elevated tubulin level in the pellet (Fig. 6D, E). As a parallel approach, we next asked how loss of DAAM affects MT stability. To this end we induced MT depolymerization by nocodazole treatment of $DAAM^{mat/zyg}$ primary neuronal cultures and compared them to control treated neurons. Control cells treated with nocodazole exhibited only a few areas along the axon which were devoid of microtubules (Fig. 6A-A' and C). In contrast, nocodazole treated $DAAM^{mat/zyg}$ primary neurons had a two fold increase in the number of brakes along axonal microtubules (Fig. 6B-B' and C). In conclusion, DAAM behaves as a potent MT stabilizing factor in two diverse assays, and its N-terminally truncated, FH1FH2 form already seems sufficient for stabilization, at least in *in vitro* conditions.

DAAM mediates the co-alignment of microtubules and actin filaments

To test the possibility of DAAM mediated coupling between MTs and F-actin, we first performed *in vitro* low speed sedimentation experiments adapted from Elie et al. 2015 (Fig. 7A-C). Phalloidin-stabilized F-actin and/or taxol-stabilized MTs were centrifuged on a sucrose cushion in the absence or presence of DAAM constructs. This strategy ensures that individual polymers (either F-actin or MTs) and F-actin bundles assembled by DAAM remain in the supernatant, only larger polymer complexes can sediment and appear in the pellet (Elie et al., 2015). Accordingly, in the presence of GST::CDAAM MTs were detected in the pellet, whereas in the presence of both F-actin and MTs a fraction of F-actin cosedimented with microtubules in the GST::CDAAM containing samples (Fig. 7C). Intrinsic to the experimental conditions, F-actin can only appear in the pellet if it is physically linked to MTs, therefore these observations imply a simultaneous interaction between CDAAM and that of the two polymer systems. In contrast to CDAAM, actin or MT polymers did not sediment in the

presence of GST::FH1-FH2 or the C-terminal DAD-CT, DAD or DAD-CT^{R-A} constructs (Fig. 7C and S4 J), suggesting that the FH2 and the CT regions are both required for F-actin and MT crosslinking yet neither is sufficient alone.

To further test the F-actin/MT coordinating ability of DAAM, TIRFM experiments were carried out with fluorescently labeled (Alexa568NHS) F-actin and MTs (labeled with HIlyte488) (Fig. 7D-F'''). For quantification the F-actin area co-localized with MTs, as well as the MT area co-localized with F-actin were derived (Elie et al., 2015) (Fig. 7G, H). In control samples lacking DAAM, ~ 13 % of F-actin and MTs appeared co-aligned (n = 19) (Fig. 7D-D'''), and the presence of GST::FH1-FH2 did not change this ratio (n = 18) (Fig. 7F-F'''). On the contrary, GST::CDAAM increased the fraction of co-aligned polymers to ~ 40 % (n = 22) (Fig. 7E-E'''), corroborating that DAAM has the ability to promote actin and MT co-alignment. In agreement with this, our actin/microtubule/DAAM colocalization studies revealed that ~22% (PPI: 0.224±0.04) of DAAM is associated with both the actin and MT cytoskeleton (Fig. 8A-D), which means that the majority of MT associated DAAM (~37%) is also colocalized to the actin cytoskeleton. Together the capacity of DAAM to simultaneously bind the two cytoskeletal systems *in vitro* and its axonal localization along the overlapping regions strongly suggest that DAAM is involved in the coordination of the actin and MT cytoskeleton.

DISCUSSION

Proper coordination of the actin and microtubule cytoskeleton is thought to be key to growth cone advance, yet the molecular mechanisms of actin-MT crosstalk during axonal growth remained largely elusive. Here we report our findings suggesting that the formin family protein DAAM is an important novel factor of actin-microtubule coordination in neuronal growth cones. Formins are extensively characterized for their ability to interact with G-actin and promote their assembly into F-actin. These studies established that the FH2 domain binds actin strongly, whereas some formins contain an additional, albeit much weaker actin binding motif in their DAD-CT region (Gould et al., 2011; Vizcarra et al., 2014). In accordance with recent findings for other formins, we found that, besides actin binding (Barko et al., 2010), the FH2 domain of DAAM is also able to interact with MTs. Moreover, we showed that the positively charged CT region but not the DAD domain is also capable of MT binding. Considering the dimeric nature of the formin proteins, the full length DAAM protein contains multiple actin and MT binding sites. However, how these interacting elements act in a concerted fashion is still elusive. The CDAAM fragment that contains all the mapped cytoskeleton interacting domains of DAAM, exhibits an F-actin bundling activity *in vitro*, and it is also able to crosslink actin filaments with MTs. In the concentration range where purified CDAAM is able to co-align F-actin and MTs, neither FH1-FH2 nor DAD-CT possesses these activities. This suggests a synergic action of these regions, for which the polymer binding ability of the FH2 domain seems to be substantial. Based on these *in vitro* data the question arises as to which of these activities are relevant *in vivo*, particularly, in growth cones. With regard to actin bundling, although not distributed uniformly, DAAM is detected along the filopodial actin bundles that would be in harmony with a role in filament bundling. Whereas majority of the DAAM protein associates either with actin filaments or with MTs, it is remarkable that a large population displays a DAAM/actin/MT triple colocalization in growth cones, possibly indicating a role in crosslinking or co-aligning. In further support of this, the effect of *DAAM* on MT dynamics and organization can also be explained by assuming that in the absence of *DAAM* the two cytoskeletal systems are decoupled from each other.

Organization of the actin and MT cytoskeleton is intimately linked to each other in most cellular processes examined. Therefore, perturbation of any of the two systems is likely to indirectly affect the other one as well. It follows that actin regulators, such as formins, may affect cellular MT organization by indirect mechanisms besides or instead of direct effects. This has so far been a relatively poorly treated, yet a critical question when studying the role

of formins in MT regulation. We attempted to address this issue by comparing the effect of an actin depolymerizing drug to the lack of DAAM in primary neurons. We found an increased MT growth speed upon Lat-A treatment in the growth cone which was very similar to what is observed in the absence of *DAAM*. However, we also noticed that Lat-A treatment induced the formation of long, filopodia-like protrusions that has never been detected in *DAAM* mutant cells. Thus it appears that partial depolymerization of the neuronal actin cytoskeleton has a comparable, yet not identical, effect on MT dynamics as to the loss of formin function, suggesting that an indirect effect cannot be excluded. Nevertheless, a number of observations argue against that the effect of DAAM on growth cone MT organization and dynamics would be exclusively or largely indirect. First, DAAM is often colocalized with MTs and it clearly has the ability to bind to MTs. Second, DAAM is able **to associate with** MTs even when its actin binding is compromised. Third, the loss of *DAAM* strongly reduces the retrograde MT translocation frequency but only weakly affects the retrograde actin flow. These results, together with that of the actin/MT crosslinking activity detected *in vitro* and the DAAM/actin/MT triple colocalization observed in growth cones, strongly suggest that the major function of DAAM is related to the coordination of actin and MT dynamics.

One intriguing characteristic of the interaction between DAAM and microtubules is the ability to bind MTs directly as well as to associate with MTs through +TIPs. The major MT related effects of DAAM, such as MT stabilization and actin-MT crosslinking, can potentially be explained by direct MT binding that would consequently impact on MT dynamics. In addition, DAAM, bound to MTs, may interact with other microtubule associated proteins that would offer further regulatory possibilities. On the other hand, +TIP binding is equally exciting, particularly in light of recently discussed models of growth cone advance (Bearce et al., 2015; Cammarata et al., 2016), and data revealing how MT plus-ends trigger formin-dependent rapid actin assembly *in vitro* and in motile cells (Henty-Ridilla et al., 2016; Jaiswal et al., 2013b; Okada et al., 2010). While in the classical models of growth cone guidance actin dynamics has been credited as the major driving force of motility and as the primary target of guidance signaling, subsequent studies suggested that the peripheral pioneer MTs also act as guidance sensors, leading to the hypothesis that the closely coupled regulation of actin and MT dynamics is at the heart of guidance signaling (Bearce et al., 2015; Cammarata et al., 2016; Coles and Bradke, 2015). Meanwhile, +TIPs, many of which are able to interact both with F-actin and MTs, were shown to act as signal transducers during growth cone guidance, and they emerged as key regulators of actin/MT coordination downstream of

axon guidance signaling. Parallel to this, it has been established that some +TIPs collaborate with the formin mDia1, that enables MT plus-ends to govern localized actin assembly *in vitro* and in fibroblast cells (Henty-Ridilla et al., 2016; Jaiswal et al., 2013b; Okada et al., 2010), and that the interaction of CLIP170 with an unknown formin is important for dendritic arbor formation in primary neurons (Henty-Ridilla et al., 2016). Given that DAAM is present at MT plus-ends and it associates with EB1 in S2 cells, we propose that DAAM is a strong candidate to promote actin assembly in concert with +TIPs. Thus, our data reinforces the importance of a formin/+TIP module as a general mechanism of linking actin and MT dynamics, and most importantly, we provide the first *in vivo* evidence that such a mechanism is at work in axonal growth cones.

In addition to the potential to promote actin polymerization at MT plus-ends, we found that DAAM retains an MT stabilizing activity both *in vitro* and in primary neurons, and the FH2 domain seems sufficient for MT stabilization. This is similar to the case of several other formins and therefore it might be a shared feature of this protein family. Although the physiological importance of formin mediated MT stabilization in the context of neuronal growth remains largely unknown, DAAM clearly appears to possess multiple capabilities to influence the cytoskeleton due to its actin nucleation and elongation, MT stabilization, MT plus end binding and actin-MT crosslinking activities. Strikingly, perhaps with the exception of actin assembly, many other +TIPs exhibit related biochemical properties. Based on this we propose that the unique or key function of DAAM in orchestrating the growth cone cytoskeleton is facilitating the formation of new actin filaments at the plus-ends of pioneer MTs (Fig. 8 E-G). We think that this step is controlled by the navigation cues which also coordinate a multitude of cytoskeletal responses, including other transient actin-MT interactions, through other actin- and/or MT-binding proteins, such as (+) TIPs, to guide axons in a complex cellular environment. Whether DAAM is an essential factor in all neurons or formins act redundantly in this context, awaits future elucidations.

MATERIALS AND METHODS

Fly stocks and genetics

For mutant analysis *DAAM^{Ex1}* or *DAAM^{Ex1};elav-Gal4,UAS-EB1::GFP* and *DAAM^{Ex68},Ubi::GFP/ Y$^{Dp(1;Y)Sz280}$* lines were crossed as described previously (Matusek et al., 2008). In addition we used the following stocks: *w^{1118}*, *w;elav-Gal4, w;UAS-DADm-DAAM::GFP* (Matusek et al. 2008), w; *UAS-CDAAM, Jupiter::GFP* (Karpova et al., 2006), w;*elav-Gal4,UAS-EB1::GFP* and *UAS-Actin5C::GFP* (Roper et al., 2005).

Molecular biology and antibody production

For S2 cell expression of ΔDAD-DAAM we used a pAWF-ΔDAD-DAAM destination clone created by standard methods. For bacterial protein expression the DAD, DAD-CT and FH1FH2^{I732A} constructs were generated by using standard cloning and *in vitro* mutagenesis methods in the pGex2T vector. The DAD-CT^{R-A} mutant construct was created by gene synthesis (Sangon Biotech), and then cloned into pGex2T (Fig. S2 F). Primers are listed in supplementary Table 1.

The novel DAAM antibody (Rb#4938) was generated in rabbit after immunization with purified FH1FH2 produced in bacteria. The sera were collected, and the IgG fraction was purified on ProteinG agarose beads. Specificity of the antibody was confirmed by Western blot analysis (Fig S3 G).

Cell cultures and immunohistochemistry

Drosophila primary neuronal cells were obtained from stage 11 embryos as published in Sanchez-Soriano et al., 2010. S2 cells were grown in Schneider's media supplemented with 10% heat inactivated FBS.

For transfection of S2 cells, 2x10^6 cells were seeded in 6-well plates and then transfected with pAct5C-ΔDAD-DAAM::3xFlag construct using Effectene transfection reagent (Qiagen).

Cultured neurons were fixed at 6 HIV, stained as described in Matusek et al., 2008. The following primary antibodies were used: mouse anti-α-tubulin (1:1000), rabbit anti-dDAAM (1:1000, Matusek et al. 2006), chicken anti-GFP (1:1000, Abcam). Actin was labelled with either Alexa-488- or Alexa-546-phalloidin (ThermoScientific).

For treatments with the microtubule destabilizing drug nocodazole, neurons were plated onto coverslips coated with 0.5 mg/ml Concanavalin A (Sigma) and kept at 22 ^{o}C for

12 h. After 12 h, neurons were treated with either nocodazole (100 uM; Sigma) or vehicle (both diluted in Schneider's medium) for 4 h at 22 ^{o}C.

Co-immunoprecipitation and Western blots

Co-immunoprecipitation was carried out as described previously (Gombos et al., 2015). Lysates of transfected S2 cells were incubated with rabbit anti-EB1 antisera, then samples were incubated with protein-A magnetic beads (Bio-Rad). Eluted proteins were analyzed by Western blot using a standard procedure. Rabbit anti-EB1 (1:2000, gift from H. Ohkura), mouse anti-Flag (1:1000, M2, Sigma-Aldrich), mouse anti-α-tubulin (1:10,000, DM1A, Sigma-Aldrich), anti-rabbit IgG-HRP (1:10000, Jackson) and anti-mouse IgG-HRP (1:5000, Dako) were used for Western blots.

Protein expression and purification

Drosophila DAAM constructs were expressed and purified as GST-tagged proteins as described (Barko et al., 2010). Actin was purified from rabbit skeletal muscle and labeled with Alexa Fluor® 568 carboxylic acid succinimidyl ester (Alexa568NHS, Invitrogen) (Kellogg et al., 1988; Spudich and Watt, 1971). Mg^{2+}-ATP-actin filaments (F-actin) and phalloidin-stabilized F-actin were prepared as described (Toth et al., 2016). Taxol-stabilized MTs were prepared from unmodified and/or HIlyte Fluor^{TM} 488 labeled tubulin (Cytoskeleton, Inc.).

MT/DAAM-binding assays

MT co-sedimentation

MTs were prepared from tubulin protein (Cytoskeleton, Inc.) following the vendor's instructions. Purified GST (4 μM) or GST-tagged dDAAM fragments (0.25 - 4 μM) were incubated with taxol-stabilized MTs (0.5 μM) for 30 min at room temperature in MT binding buffer (MBB;10 mM HEPES pH 7.0, 1 mM $MgCl_2$, 1 mM EGTA, 1 mM DTT, 20 μM taxol, 0.5 mM thesit). Samples were centrifuged at 100,000 g for 25 min. The pellets were washed in MBB then resuspended in SDS-PAGE sample buffer. Proteins in the supernatants and pellets were resolved by SDS-PAGE and stained by colloidal Coomassie blue.

GST pull-down assay

GST and GST-tagged DAAM fragments were expressed and purified from a small volume culture (2 mL) as described above. The proteins were not eluted from glutathione beads, instead the beads were incubated with pre-assembled MTs (0.5 μM) for 30 min in MBB. Beads were washed in MBB then the proteins were eluted and analyzed by SDS-PAGE and Western blot.

MT stability assay

The cold-induced depolymerization assay was carried out as described (Bartolini et al., 2008). Tubulin was polymerized in the presence of 4 μM GST or GST::FH1FH2 proteins. After polymerization matching aliquots of samples were centrifuged as described for MT co-sedimentation. The remaining samples were incubated on ice, then centrifuged at 4 °C. Proteins in the supernatants and pellets were resolved by Coomassie-stained SDS-PAGE and the gels were quantified by using densitometry (ImageJ).

MT/F-actin crosslinking assay

Since both CDAAM and FH1-FH2 induces F-actin bundles, which sediment at very low speed, we adapted the sedimentation protocol used by Elie et al 2015 to test the ability of DAAM to interact simultaneously with F-actin and MTs. Phalloidin-stabilized F-actin (2 μM) and/or taxol-stabilized MTs (2 μM) were incubated with DAAM constructs (9 μM) in BRB-K at room temperature for 40 min. Samples were loaded onto a 30 % sucrose cushion and centrifuged (4000 g, 10 min, 25^{o}C). Under these conditions individual polymers, as well as F-actin bundles do not sediment, only larger filament complexes (MT bundles, MT-F-actin copolymers) appear in the pellet (Elie et al., 2015). Pellets and supernatants were analyzed by SDS-PAGE. In control experiments based on high-speed centrifugation (100.000 g, 20 min, 25^{o}C) both F-actin and MTs appeared in the pellet, which confirms that both polymers exist under the applied experimental conditions, and the lack of sedimentation of the polymers is not due to depolymerization.

Microscopy and image analysis

Confocal images were captured either on a Zeiss LSM880 or on an Olympus FV1000 LSM. Images were restored using the Huygens Professional software (Scientific Volume Imaging). To visualize the F-actin and MT structures induced by DAAM, phalloidin-stabilized F-actin (0.4 μM containing 10 % Alexa568NHS-actin) and taxol-stabilized MTs (0.4 μM containing 10 % HIlyte Fluor^{TM} 488-tubulin) were incubated with DAAM constructs (1 μM) in BRB-K

at room temperature for 30 min. Samples were diluted in BRB-K* (BRB-K supplemented with 0.2 % (w/v) methylcellulose, 0.5 % (w/v) BSA, 50 mM 1,4-diazabicyclo-[2,2,2]octane (DABCO) and 100 mM DTT), applied onto poly-L-lysine-treated (Sigma Aldrich) coverslips and visualized by TIRF microscopy (Olympus IX 81). Microtubule-F-actin co-localization was quantified as described (Elie et al., 2015) (3 – 4 independent experiments at each conditions, 18-22 images). For nocodazole treatment in primary neurons, images were captured with a Nikon Eclipse 90i microscope equipped with a high resolution CCD Camera (Retiga 3000). Images were processed using ImageJ software.

MT dynamics were analyzed from EB1::GFP time lapse recordings, using TrackMate (v3.3.0). To allow particle detection and faithful tracking the spatial and temporal resolution of the live recordings were set to 100 nm/voxel and 0.9 sec/frame, respectively. Filopodial actin dynamics measurements were performed on 7-9 HIV neurons expressing Actin5C::GFP. Imaging of the neurons was performed in glass bottom petri dishes (MatTek corporation) in growth media. Filopodia with recognizable extension and retraction events were selected for further analysis.

Statistics and figures

Statistical analysis was carried out using Prism 5 (GraphPad Software Inc.). D'Agostino-Pearson omnibus test was used to assess the normality of the data. Pairwise comparisons were made using either the Student's t test or the Mann-Whitney U test according to the normality. ANOVA was used for multiple comparisons; $p<0.05$ was considered as statistically significant. Figures and cartoons were edited in Illustrator CS4 (Adobe).

ACKNOWLEDGEMENTS

We thank the Bloomington Stock Center, Hiro Ohkura and Andreas Prokop for fly stocks and reagents. We thank Éva Monostori for help with antibody production, and Anikó Berente, Edit Gyáni and Anna Rehák for technical assistance.

COMPETING INTERESTS

No competing interests declared.

AUTHOR CONTRIBUTIONS

P.H., B.B. and J.M. conceived and supervised the study; S.S., I.F., K.T., E.M.,A.V., B.B., **P.K**. and J.M. performed the experiments; S.S., I.F., B.B., **N.S.S.** and J.M. analyzed data; S.S., I.F., B.B. and J.M. wrote the manuscript.

FUNDING

This work was supported by the Hungarian Science Foundation (OTKA) (K109330 to J.M., K109689 to B.B.), the Hungarian Brain Research Program (KTIA_NAP_13-2-2014-0007 to J.M.), the National Research, Development and Innovation Office (GINOP-2.3.2-15-2016-00001 and GINOP-2.3.2-15-2016-00032 to J.M.), the European Union and the State of Hungary, co-financed by the European Social Fund in the framework of TÁMOP 4.2.4.A/2-11-1-2012-0001 'National Excellence Program' and the New National Excellence Program of the Ministry of Human Capacities (to B.B.), the ÚNKP-16-4 New National Excellence Program of the Ministry of Human Capacities (to B.B.), the Biotechnology and Biological Sciences Research Council, BBSRC (BB/M007456/1 to N.S.S) and by an MTA Postdoctoral Fellowship (to I.F.) and by the University of Liverpool and University of Szeged (Studentship to P.K.).

REFERENCES

Alberts, A. S. (2001). Identification of a carboxyl-terminal diaphanous-related formin homology protein autoregulatory domain. *J Biol Chem* **276**, 2824-30.

Barko, S., Bugyi, B., Carlier, M. F., Gombos, R., Matusek, T., Mihaly, J. and Nyitrai, M. (2010). Characterization of the biochemical properties and biological function of the formin homology domains of Drosophila DAAM. *J Biol Chem* **285**, 13154-69.

Bartolini, F. and Gundersen, G. G. (2010). Formins and microtubules. *Biochim Biophys Acta* **1803**, 164-73.

Bartolini, F., Moseley, J. B., Schmoranzer, J., Cassimeris, L., Goode, B. L. and Gundersen, G. G. (2008). The formin mDia2 stabilizes microtubules independently of its actin nucleation activity. *J Cell Biol* **181**, 523-36.

Bearce, E. A., Erdogan, B. and Lowery, L. A. (2015). TIPsy tour guides: how microtubule plus-end tracking proteins (+TIPs) facilitate axon guidance. *Front Cell Neurosci* **9**, 241.

Bornschlogl, T., Romero, S., Vestergaard, C. L., Joanny, J. F., Van Nhieu, G. T. and Bassereau, P. (2013). Filopodial retraction force is generated by cortical actin dynamics and controlled by reversible tethering at the tip. *Proc Natl Acad Sci U S A* **110**, 18928-33.

Buck, K. B. and Zheng, J. Q. (2002). Growth cone turning induced by direct local modification of microtubule dynamics. *J Neurosci* **22**, 9358-67.

Burnette, D. T., Schaefer, A. W., Ji, L., Danuser, G. and Forscher, P. (2007). Filopodial actin bundles are not necessary for microtubule advance into the peripheral domain of Aplysia neuronal growth cones. *Nat Cell Biol* **9**, 1360-9.

Cammarata, G. M., Bearce, E. A. and Lowery, L. A. (2016). Cytoskeletal social networking in the growth cone: How +TIPs mediate microtubule-actin cross-linking to drive axon outgrowth and guidance. *Cytoskeleton (Hoboken)* **73**, 461-76.

Cheng, L., Zhang, J., Ahmad, S., Rozier, L., Yu, H., Deng, H. and Mao, Y. (2011). Aurora B regulates formin mDia3 in achieving metaphase chromosome alignment. *Dev Cell* **20**, 342-52.

Chesarone, M. A., DuPage, A. G. and Goode, B. L. (2010). Unleashing formins to remodel the actin and microtubule cytoskeletons. *Nat Rev Mol Cell Biol* **11**, 62-74.

Coles, C. H. and Bradke, F. (2015). Coordinating neuronal actin-microtubule dynamics. *Curr Biol* **25**, R677-91.

Coue, M., Brenner, S. L., Spector, I. and Korn, E. D. (1987). Inhibition of actin polymerization by latrunculin A. *FEBS Lett* **213**, 316-8.

Dahlgaard, K., Raposo, A. A., Niccoli, T. and St Johnston, D. (2007). Capu and Spire assemble a cytoplasmic actin mesh that maintains microtubule organization in the Drosophila oocyte. *Dev Cell* **13**, 539-53.

Dent, E. W. and Gertler, F. B. (2003). Cytoskeletal dynamics and transport in growth cone motility and axon guidance. *Neuron* **40**, 209-27.

Dent, E. W. and Kalil, K. (2001). Axon branching requires interactions between dynamic microtubules and actin filaments. *J Neurosci* **21**, 9757-69.

Elie, A., Prezel, E., Guerin, C., Denarier, E., Ramirez-Rios, S., Serre, L., Andrieux, A., Fourest-Lieuvin, A., Blanchoin, L. and Arnal, I. (2015). Tau co-organizes dynamic microtubule and actin networks. *Sci Rep* **5**, 9964.

Forscher, P. and Smith, S. J. (1988). Actions of cytochalasins on the organization of actin filaments and microtubules in a neuronal growth cone. *J Cell Biol* **107**, 1505-16.

Gaillard, J., Ramabhadran, V., Neumanne, E., Gurel, P., Blanchoin, L., Vantard, M. and Higgs, H. N. (2011). Differential interactions of the formins INF2, mDia1, and mDia2 with microtubules. *Mol Biol Cell* **22**, 4575-87.

Gasteier, J. E., Schroeder, S., Muranyi, W., Madrid, R., Benichou, S. and Fackler, O. T. (2005). FHOD1 coordinates actin filament and microtubule alignment to mediate cell elongation. *Exp Cell Res* **306**, 192-202.

Gombos, R., Migh, E., Antal, O., Mukherjee, A., Jenny, A. and Mihaly, J. (2015). The Formin DAAM Functions as Molecular Effector of the Planar Cell Polarity Pathway during Axonal Development in Drosophila. *J Neurosci* **35**, 10154-67.

Goncalves-Pimentel, C., Gombos, R., Mihaly, J., Sanchez-Soriano, N. and Prokop, A. (2011). Dissecting regulatory networks of filopodia formation in a Drosophila growth cone model. *PLoS One* **6**, e18340.

Gould, C. J., Maiti, S., Michelot, A., Graziano, B. R., Blanchoin, L. and Goode, B. L. (2011). The Formin DAD Domain Plays Dual Roles in Autoinhibition and Actin Nucleation. *Current Biology* **21**, 384-390.

Henty-Ridilla, J. L., Rankova, A., Eskin, J. A., Kenny, K. and Goode, B. L. (2016). Accelerated actin filament polymerization from microtubule plus ends. *Science* **352**, 1004-9.

Higashida, C., Miyoshi, T., Fujita, A., Oceguera-Yanez, F., Monypenny, J., Andou, Y., Narumiya, S. and Watanabe, N. (2004). Actin polymerization-driven molecular movement of mDia1 in living cells. *Science* **303**, 2007-10.

Jaiswal, R., Breitsprecher, D., Collins, A., Correa, I. R., Jr., Xu, M. Q. and Goode, B. L. (2013a). The formin Daam1 and fascin directly collaborate to promote filopodia formation. *Curr Biol* **23**, 1373-9.

Jaiswal, R., Stepanik, V., Rankova, A., Molinar, O., Goode, B. L. and McCartney, B. M. (2013b). Drosophila homologues of adenomatous polyposis coli (APC) and the formin diaphanous collaborate by a conserved mechanism to stimulate actin filament assembly. *J Biol Chem* **288**, 13897-905.

Jiang, K., Toedt, G., Montenegro Gouveia, S., Davey, N. E., Hua, S., van der Vaart, B., Grigoriev, I., Larsen, J., Pedersen, L. B., Bezstarosti, K. et al. (2012). A Proteome-wide screen for mammalian SxIP motif-containing microtubule plus-end tracking proteins. *Curr Biol* **22**, 1800-7.

Karpova, N., Bobinnec, Y., Fouix, S., Huitorel, P. and Debec, A. (2006). Jupiter, a new Drosophila protein associated with microtubules. *Cell Motil Cytoskeleton* **63**, 301-12.

Kellogg, D. R., Mitchison, T. J. and Alberts, B. M. (1988). Behaviour of microtubules and actin filaments in living Drosophila embryos. *Development* **103**, 675-86.

Komarova, Y., De Groot, C. O., Grigoriev, I., Gouveia, S. M., Munteanu, E. L., Schober, J. M., Honnappa, S., Buey, R. M., Hoogenraad, C. C., Dogterom, M. et al. (2009). Mammalian end binding proteins control persistent microtubule growth. *J Cell Biol* **184**, 691-706.

Kovar, D. R. and Pollard, T. D. (2004). Insertional assembly of actin filament barbed ends in association with formins produces piconewton forces. *Proc Natl Acad Sci U S A* **101**, 14725-30.

Lewkowicz, E., Herit, F., Le Clainche, C., Bourdoncle, P., Perez, F. and Niedergang, F. (2008). The microtubule-binding protein CLIP-170 coordinates mDia1 and actin reorganization during CR3-mediated phagocytosis. *J Cell Biol* **183**, 1287-98.

Li, F. and Higgs, H. N. (2003). The mouse Formin mDia1 is a potent actin nucleation factor regulated by autoinhibition. *Curr Biol* **13**, 1335-40.

Li, F. and Higgs, H. N. (2005). Dissecting requirements for auto-inhibition of actin nucleation by the formin, mDia1. *J Biol Chem* **280**, 6986-92.

Liu, W., Sato, A., Khadka, D., Bharti, R., Diaz, H., Runnels, L. W. and Habas, R. (2008). Mechanism of activation of the Formin protein Daam1. *Proc Natl Acad Sci U S A* **105**, 210-5.

Lowery, L. A. and Van Vactor, D. (2009). The trip of the tip: understanding the growth cone machinery. *Nat Rev Mol Cell Biol* **10**, 332-43.

Marx, A., Godinez, W. J., Tsimashchuk, V., Bankhead, P., Rohr, K. and Engel, U. (2013). Xenopus cytoplasmic linker-associated protein 1 (XCLASP1) promotes axon elongation and advance of pioneer microtubules. *Mol Biol Cell* **24**, 1544-58.

Matusek, T., Djiane, A., Jankovics, F., Brunner, D., Mlodzik, M. and Mihaly, J. (2006). The Drosophila formin DAAM regulates the tracheal cuticle pattern through organizing the actin cytoskeleton. *Development* **133**, 957-66.

Matusek, T., Gombos, R., Szecsenyi, A., Sanchez-Soriano, N., Czibula, A., Pataki, C., Gedai, A., Prokop, A., Rasko, I. and Mihaly, J. (2008). Formin proteins of the DAAM subfamily play a role during axon growth. *J Neurosci* **28**, 13310-9.

Meijering, E., Jacob, M., Sarria, J. C., Steiner, P., Hirling, H. and Unser, M. (2004). Design and validation of a tool for neurite tracing and analysis in fluorescence microscopy images. *Cytometry A* **58**, 167-76.

Morrison, E. E., Moncur, P. M. and Askham, J. M. (2002). EB1 identifies sites of microtubule polymerisation during neurite development. *Brain Res Mol Brain Res* **98**, 145-52.

Okada, K., Bartolini, F., Deaconescu, A. M., Moseley, J. B., Dogic, Z., Grigorieff, N., Gundersen, G. G. and Goode, B. L. (2010). Adenomatous polyposis coli protein nucleates actin assembly and synergizes with the formin mDia1. *J Cell Biol* **189**, 1087-96.

Otomo, T., Otomo, C., Tomchick, D. R., Machius, M. and Rosen, M. K. (2005). Structural basis of Rho GTPase-mediated activation of the formin mDia1. *Mol Cell* **18**, 273-81.

Roper, K., Mao, Y. and Brown, N. H. (2005). Contribution of sequence variation in Drosophila actins to their incorporation into actin-based structures in vivo. *J Cell Sci* **118**, 3937-48.

Rosales-Nieves, A. E., Johndrow, J. E., Keller, L. C., Magie, C. R., Pinto-Santini, D. M. and Parkhurst, S. M. (2006). Coordination of microtubule and microfilament dynamics by Drosophila Rho1, Spire and Cappuccino. *Nat Cell Biol* **8**, 367-76.

Rose, R., Weyand, M., Lammers, M., Ishizaki, T., Ahmadian, M. R. and Wittinghofer, A. (2005). Structural and mechanistic insights into the interaction between Rho and mammalian Dia. *Nature* **435**, 513-8.

Roth-Johnson, E. A., Vizcarra, C. L., Bois, J. S. and Quinlan, M. E. (2014). Interaction between microtubules and the Drosophila formin Cappuccino and its effect on actin assembly. *J Biol Chem* **289**, 4395-404.

Sagot, I., Rodal, A. A., Moseley, J., Goode, B. L. and Pellman, D. (2002). An actin nucleation mechanism mediated by Bni1 and profilin. *Nat Cell Biol* **4**, 626-31.

Sanchez-Soriano, N., Goncalves-Pimentel, C., Beaven, R., Haessler, U., Ofner-Ziegenfuss, L., Ballestrem, C. and Prokop, A. (2010). Drosophila growth cones: a genetically tractable platform for the analysis of axonal growth dynamics. *Dev Neurobiol* **70**, 58-71.

Schaefer, A. W., Kabir, N. and Forscher, P. (2002). Filopodia and actin arcs guide the assembly and transport of two populations of microtubules with unique dynamic parameters in neuronal growth cones. *J Cell Biol* **158**, 139-52.

Schaefer, A. W., Schoonderwoert, V. T., Ji, L., Mederios, N., Danuser, G. and Forscher, P. (2008). Coordination of actin filament and microtubule dynamics during neurite outgrowth. *Dev Cell* **15**, 146-62.

Schonichen, A. and Geyer, M. (2010). Fifteen formins for an actin filament: a molecular view on the regulation of human formins. *Biochim Biophys Acta* **1803**, 152-63.

Shaye, D. D. and Greenwald, I. (2015). The disease-associated formin INF2/EXC-6 organizes lumen and cell outgrowth during tubulogenesis by regulating F-actin and microtubule cytoskeletons. *Dev Cell* **32**, 743-55.

Spudich, J. A. and Watt, S. (1971). The regulation of rabbit skeletal muscle contraction. I. Biochemical studies of the interaction of the tropomyosin-troponin complex with actin and the proteolytic fragments of myosin. *J Biol Chem* **246**, 4866-71.

Stepanova, T., Slemmer, J., Hoogenraad, C. C., Lansbergen, G., Dortland, B., De Zeeuw, C. I., Grosveld, F., van Cappellen, G., Akhmanova, A. and Galjart, N. (2003). Visualization of microtubule growth in cultured neurons via the use of EB3-GFP (end-binding protein 3-green fluorescent protein). *J Neurosci* **23**, 2655-64.

Tinevez, J. Y., Perry, N., Schindelin, J., Hoopes, G. M., Reynolds, G. D., Laplantine, E., Bednarek, S. Y., Shorte, S. L. and Eliceiri, K. W. (2016). TrackMate: An open and extensible platform for single-particle tracking. *Methods*.

Toth, M. A., Majoros, A. K., Vig, A. T., Migh, E., Nyitrai, M., Mihaly, J. and Bugyi, B. (2016). Biochemical Activities of the Wiskott-Aldrich Syndrome Homology Region 2 Domains of Sarcomere Length Short (SALS) Protein. *J Biol Chem* **291**, 667-80.

Vizcarra, C. L., Bor, B. and Quinlan, M. E. (2014). The role of formin tails in actin nucleation, processive elongation, and filament bundling. *J Biol Chem* **289**, 30602-13.

Watanabe, N. and Higashida, C. (2004). Formins: processive cappers of growing actin filaments. *Exp Cell Res* **301**, 16-22.

Waterman-Storer, C. M. and Salmon, E. D. (1998). How microtubules get fluorescent speckles. *Biophys J* **75**, 2059-69.

Wen, Y., Eng, C. H., Schmoranzer, J., Cabrera-Poch, N., Morris, E. J., Chen, M., Wallar, B. J., Alberts, A. S. and Gundersen, G. G. (2004). EB1 and APC bind to mDia to stabilize microtubules downstream of Rho and promote cell migration. *Nat Cell Biol* **6**, 820-30.

Wu, Y., Eghbali, M., Ou, J., Lu, R., Toro, L. and Stefani, E. (2010). Quantitative determination of spatial protein-protein correlations in fluorescence confocal microscopy. *Biophys J* **98**, 493-504.

Yarmola, E. G., Somasundaram, T., Boring, T. A., Spector, I. and Bubb, M. R. (2000). Actin-latrunculin A structure and function. Differential modulation of actin-binding protein function by latrunculin A. *J Biol Chem* **275**, 28120-7.

Young, K. G. and Copeland, J. W. (2010). Formins in cell signaling. *Biochim Biophys Acta* **1803**, 183-90.

Young, K. G., Thurston, S. F., Copeland, S., Smallwood, C. and Copeland, J. W. (2008). INF1 is a novel microtubule-associated formin. *Mol Biol Cell* **19**, 5168-80.

Zhou, F., Leder, P. and Martin, S. S. (2006). Formin-1 protein associates with microtubules through a peptide domain encoded by exon-2. *Exp Cell Res* **312**, 1119-26.

Zhou, F. Q. and Cohan, C. S. (2004). How actin filaments and microtubules steer growth cones to their targets. *J Neurobiol* **58**, 84-91.

Zinchuk, V., Wu, Y., Grossenbacher-Zinchuk, O. and Stefani, E. (2011). Quantifying spatial correlations of fluorescent markers using enhanced background reduction with protein proximity index and correlation coefficient estimations. *Nat Protoc* **6**, 1554-67.

FIGURE LEGENDS

Figure 1. Axonal localization and physical interaction of DAAM with microtubules.

(**A-D**) Growth cone of a primary neuron (6 HIV), labeled against F-actin, tubulin and DAAM. Asterisk marks filopodial DAAM localization. Arrows point to DAAM puncta localized at the end of microtubules. **Arrowheads show DAAM localization along the MT bundles.** (**E**) Scatterplots show the protein-protein proximity index measured between DAAM and F-actin, and DAAM and tubulin. Grey dots represent values measured on individual cells (DAAM-Actin, 0.46±0.14, mean±s.d. n=40; DAAM-Tubulin, 0.38±0.15, mean±s.d. n=40). Black dots represent the median of the independent experiments with their median. (**F**) Bar diagram shows the frequency of microtubule end localization of DAAM (36.18 % ±13.57 %, mean±s.d.; measured on **100 MT ends** from three independent experiments). (**G**) Domain structure of full length DAAM and DAAM fragments used in this study. (**H**) **MT co-sedimentation assay shows that MTs physically interact with the FH1FH2 fragment of dDAAM.** (**I**) Co-IP shows that ΔDAD-DAAM::3xFlag co-precipitates specifically with EB1 from S2 cell lysates.

Figure 2. DAAM affects axonal microtubule length and morphology.

(**A-D**) Representative images of primary neurons (6 HIV) derived from wild type (*white*^{1118}) (**A, A'**), *DAAM*$^{mat/zyg}$ (see materials and methods) (**B, B'**), *Elav-Gal4* (*w;elav-Gal4/+*)(**C, C'**) or *CDAAM* (*w;elav-Gal4,UAS-CDAAM/+*) (**D, D'**) expressing embryos. (**E**) Examples for classification of growth cone microtubules as bundled, looped or spread. (**F**) Scatterplots show the length of the axonal microtubules of primary neurons. Grey dots represent values measured on individual cells (wild type: 15.42 μm, n=235; *DAAM*$^{mat/zyg}$: 9.61 μm, n=152; *Elav-Gal4*: 20.3 μm, n=182; *CDAAM*: 13.8 μm, n=178; median with interquartile range). Black dots represent the median of the independent experiments with their median. (**G**) Boxplots show the frequency of axonal microtubule morphology classes. Unpaired *t*-tests were used for statistical analysis.

Figure 3. The effect of DAAM on axonal microtubule dynamics.

(**A**) Representative image of a primary neuron expressing EB1::GFP (6 HIV) (time-lapse projection). The axon and the growth cone are distinguished by dotted rectangles. (**B**) Time-lapse projection of recognized EB1::GFP tracks. The tracks are color coded according to their median velocity (from yellow to cyan, 0 μm×min^{-1} – 30 μm×min^{-1}). (**C**) Scatterplots show

significant velocity difference between the axonal and growth cone EB1::GFP comets (growth cone: 6.54 μm×min^{-1}, n=64; axon: 8.12 μm×min^{-1}, n=60; median with interquartile range). (**D**) Scatterplots show the median velocity of EB1::GFP tracks measured on primary neurons derived from EB1::GFP expressing wild type and *DAAM*$^{mat/zyg}$ embryos. It is also compared to EB1::GFP expressing wild type neurons treated with latrunculin A (growth cone - wild type: 6.54 μm×min^{-1}, n=64; *DAAM*$^{mat/zyg}$: 12.53 μm×min^{-1}, n=57; latrunculin A treated: 11.16 μm×min^{-1}, n=18) (axon - wild type: 8.12 μm×min^{-1}, n=60; *DAAM*$^{mat/zyg}$: 14.64 μm×min^{-1}, n=52; latrunculin A treated: 13.85 μm×min^{-1}, n=15; median with interquartile range). Dots represent the median velocity of the EB1::GFP tracks measured on individual cells. Mann Whitney test was used to compare the respective pairs. (**E**) Survival analysis was used to compare microtubule lifetime of wild type and *DAAM*$^{mat/zyg}$ neurons expressing EB1::GFP. Short tracks (below 3.6 second) were discarded from the analysis and the threshold is marked with a dotted line. The Mantel-Cox test was used to compare the survival curves (white, n=219; *DAAM*$^{mat/zyg}$, n=161).

Figure 4. The effect of DAAM on retrograde MT translocation

(**A**) The cartoon illustrates a growth cone filopodia invaded by a microtubule where the growing plus end is labeled with EB1::GFP. (**B-C'**) Representative kymographs demonstrate microtubule plus end displacement along growth cone filopodia in wild type (**B, B'**) and *DAAM*$^{mat/zyg}$ (**C, C'**) neurons expressing EB1::GFP. Red arrowheads mark the point where microtubules stall or undergo retrograde translocation. Dotted lines indicate where pioneer microtubules enter the growth cone filopodia. (**D**) Boxplot shows the frequency of microtubule retrograde translocation in wild type and *DAAM*$^{mat/zyg}$ neurons (*white*: 18.9 ± 6.4, n=219; *DAAM*$^{mat/zyg}$: 6.3 ±2.5, n=161; mean ± s.d, from four independent experiments). (**E-F'**) Summary of extracted kymographs from wild type (**E**) and *DAAM*$^{mat/zyg}$ (**F**) neurons expressing EB1::GFP. (**E', F'**) Histograms show the summarized directionality distribution, measured on the extracted kymographs.

Figure 5. Effect of DAAM on axonal filopodia and actin dynamics.

(**A**) A cartoon to illustrate filopodia dynamics (extension and retraction) and the underlying actin dynamics (actin polymerization, retrograde flow). (**B, C**) Axons of Actin5C::GFP expressing (**B**) wild type and (**C**) *DAAM*$^{mat/zyg}$ neurons (6 HIV). The growth cones are marked by a dotted red circle. (**D**) Filopodia with unevenly incorporated Actin5C::GFP; Scale bar: 200nm. (**D'**) A kymograph revealing the actin retrograde flow meanwhile the filopodia

extends and retracts. (**E-G**) Scatterplots show filopodia extension (wild type: 5.28 μm×min^{-1}, n=134; *DAAM*$^{mat/zyg}$: 6.75 μm×min^{-1}, n=64), retraction (wild type: 6.82 μm×min^{-1}, n=91; *DAAM*$^{mat/zyg}$: 3.38 μm×min^{-1}, n=117) and actin retrograde flow (wild type: 5.64 μm×min^{-1}, n=114; *DAAM*$^{mat/zyg}$: 2.93 μm×min^{-1}, n=97) rates measured in wild type and *DAAM*$^{mat/zyg}$ neurons expressing Actin5C::GFP. Grey dots represent the values of individual events. Black dots represent the median of independent experiments. Mann Whitney test was applied for statistical analysis. (**H**) Scheme of a hypothetical kymograph recorded along filopodia depicted on panel A. (**I, J**) Scatterplots show actin plus end dynamics during filopodia extension (wild type: 5.28 μm×min^{-1}, n=134; *DAAM*$^{mat/zyg}$: 6.75 μm×min^{-1}, n=64) and retraction rates (wild type: 6.82 μm×min^{-1}, n=91; *DAAM*$^{mat/zyg}$: 3.38 μm×min^{-1}, n=117) measured in wild type and *DAAM*$^{mat/zyg}$ neurons expressing Actin5C::GFP. Grey dots represent the values of individual events calculated based on the actin retrograde flow and filopodia extension and retraction rates.

Figure 6. DAAM stabilizes MTs *in vivo* and *in vitro*

(A-B') Images show axonal MT bundles of DMSO (A, B) or nocodazole (A', B') treated control and *DAAM*$^{mat/zyg}$ primary neurons (12 HIV). Arrows point to gaps along axonal MT bundles. (C) Quantification of the number of breaks along the MT bundles of control (DMSO treated: 1±0.2, mean±s.e.m., n=213; nocodazole treated: 6.7±0.8, mean±s.e.m., n=206) and *DAAM*$^{mat/zyg}$ primary (DMSO treated: 2.3±0.4, mean±s.e.m., n=157; nocodazole treated: 12±1.3, mean±s.e.m., n=137) neurons, measured in 3 independent experiments. (D, E) Densitometric analysis of SDS-PAGE gels (D) show that the amount of tubulin in the pellet is higher in samples with GST::FH1FH2 (E) after cold-induced depolymerization as compared to controls (mean±s.d., n=3, ** P<0.01).

Figure 7. F-actin and microtubule co-alignment mediated by DAAM.

(**A-C**) Representative Coomassie-stained SDS-PAGE gels from low-speed centrifugation experiments showing the amount of MTs and F-actin in the supernatants (S) and in the pellets (P) in the absence or presence of either GST::CDAAM or FH1-FH2, as indicated. (**D-F**) Representative fluorescence micrographs of F-actin (cyan) and MTs (red) in the absence or presence of GST::CDAAM and GST::FH1FH2, as indicated. Yellow regions on the merged images highlight the overlapping F-actin and MT regions. Binary images show the overlapping polymer area. (**G, H**) Ratio of the co-aligned F-actin and MT area in the absence

or presence of GST::CDAAM or GST::FH1FH2 (average of 3–4 independent experiments is shown).

Figure 8. DAAM colocalizes with overlapping F-actin and microtubules.

(**A-D**) A representative growth cone showing DAAM puncta on overlapping F-actin and MTs (white rectangle). (**B**) The yellow dotted line marks the outline of the growth cone. (**C**) Image shows microtubules (red) and microtubules overlapping with actin filaments (grey). Inlet shows DAAM puncta (magenta) localized on overlapping F-actin and microtubules. (**D**) Scatterplots show the protein-protein proximity index measured between DAAM and the overlapping F-actin and microtubules. Grey dots represent values measured on individual cells (0.22±0.1, mean±s.d. n=40). Black dots represent the median of the independent experiments with their median. **(E) Schematic model of the growth cone cytoskeleton. (F, G) Localization and proposed functions of DAAM in growth cones based on former studies and the current study: 1) actin barbed end binding, actin assembly, 2) F-actin bundling, 3) MT side binding (stabilization), 4) EB1 binding, 5) F-actin and MT coalignment. Our current work suggests that the key function of DAAM is to facilitate/boost the formation of new actin filaments at the MT plus-ends through interactions with EB1.**

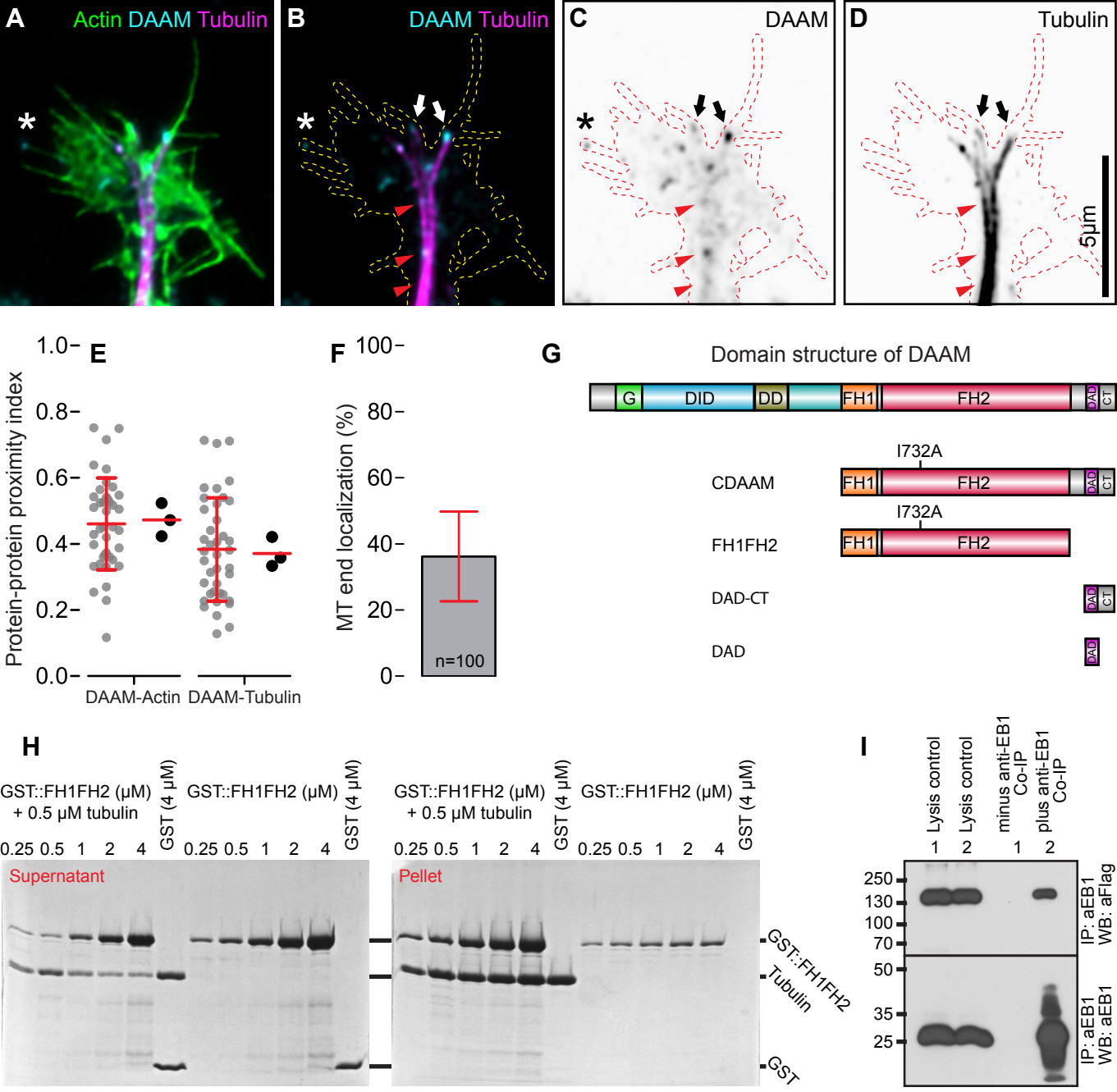
A
Actin DAAM Tubulin
B
DAAM Tubulin
C
DAAM
D
Tubulin
5µm
E
Protein-protein proximity index
1.0
0.8
0.6
0.4
0.2
0.0
DAAM-Actin
DAAM-Tubulin
F
MT end localization (%)
100
80
60
40
20
0
n=100
G
Domain structure of DAAM
G
DID
DD
FH1
FH2
DAD
CT
CDAAM
I732A
FH1FH2
DAD-CT
DAD
H
GST::FH1FH2 (µM)
+ 0.5 µM tubulin
GST (4 µM)
0.25 0.5 1 2 4
Supernatant
Pellet
GST::FH1FH2
Tubulin
GST
I
Lysis control
minus anti-EB1 Co-IP
plus anti-EB1 Co-IP
1 2 1 2
250
130
100
70
50
35
25
IP: aEB1
WB: aFlag
IP: aEB1
WB: aEB1

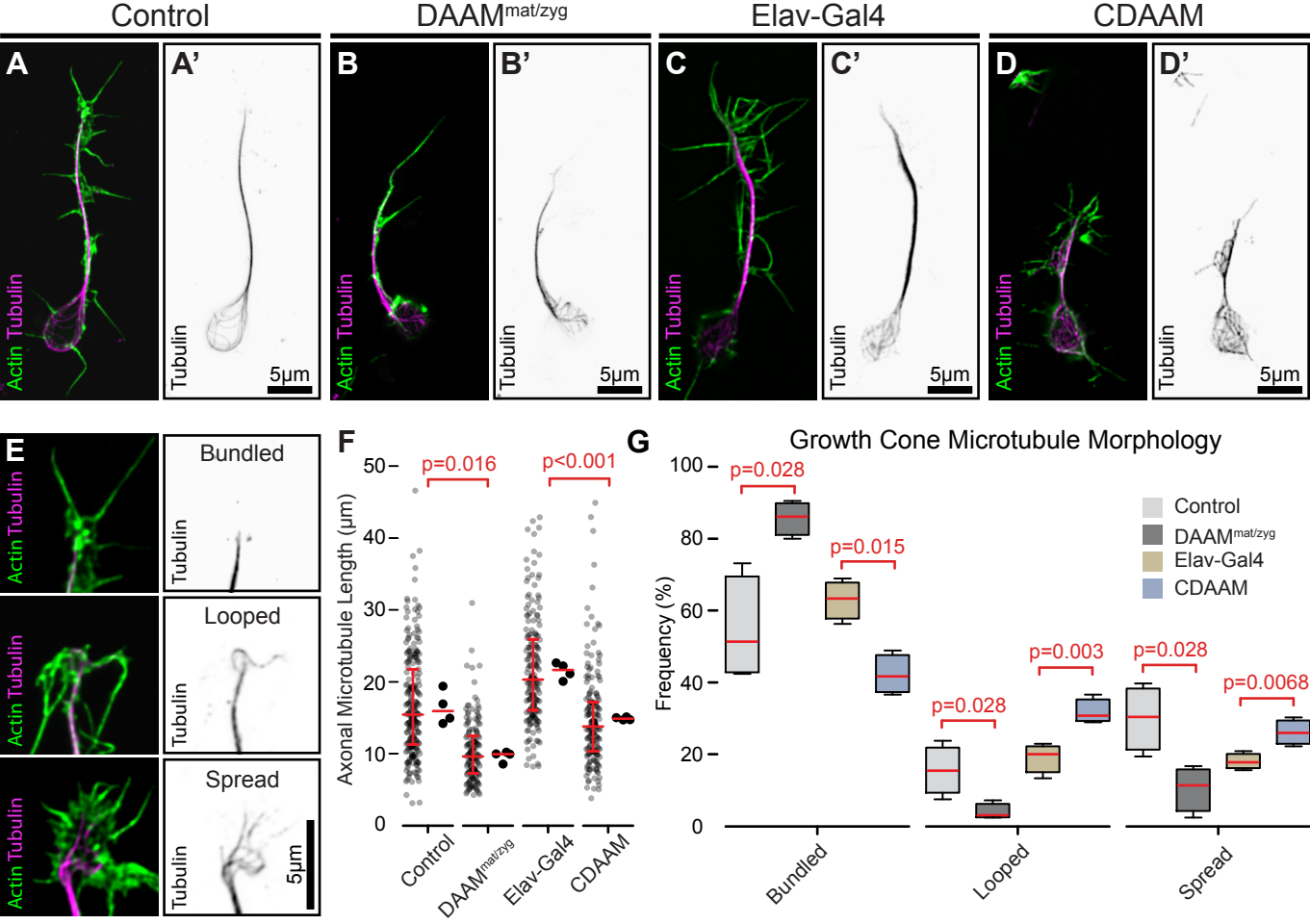
Control
DAAMmat/zyg
Elav-Gal4
CDAAM
A
A'
B
B'
C
C'
D
D'
Actin Tubulin
Tubulin
5µm
E
Bundled
Looped
Spread
F
Axonal Microtubule Length (µm)
p=0.016
p<0.001
Control
DAAMmat/zyg
Elav-Gal4
CDAAM
G
Growth Cone Microtubule Morphology
Frequency (%)
p=0.028
p=0.015
p=0.028
p=0.003
p=0.028
p=0.0068
Bundled
Looped
Spread

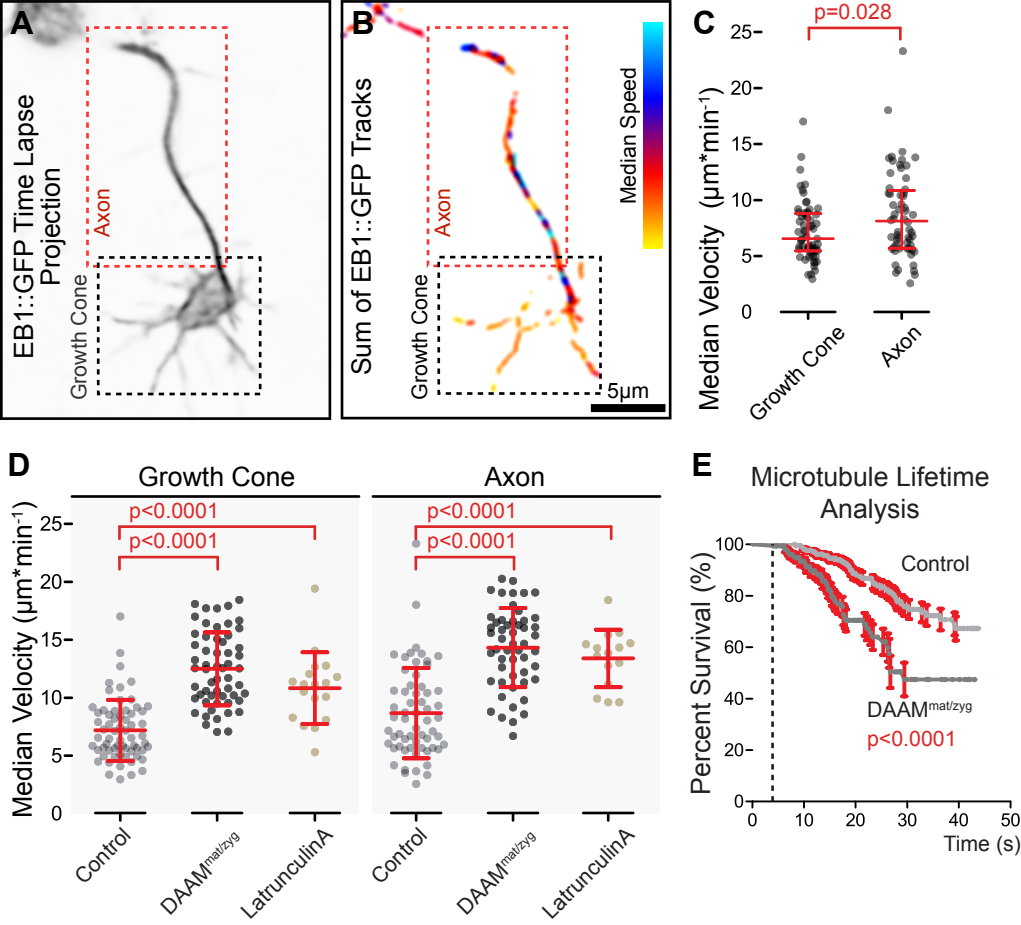
A
EB1::GFP Time Lapse Projection
Axon
Growth Cone
B
Sum of EB1::GFP Tracks
Median Speed
Axon
Growth Cone
5µm
C
p=0.028
Median Velocity (µm*min-1)
25
20
15
10
5
0
Growth Cone
Axon
D
Growth Cone
Axon
Median Velocity (µm*min-1)
p<0.0001
p<0.0001
p<0.0001
p<0.0001
25
20
15
10
5
0
Control
DAAMmat/zyg
LatrunculinA
Control
DAAMmat/zyg
LatrunculinA
E
Microtubule Lifetime Analysis
Percent Survival (%)
100
80
60
40
20
0
Control
DAAMmat/zyg
p<0.0001
0
10
20
30
40
50
Time (s)

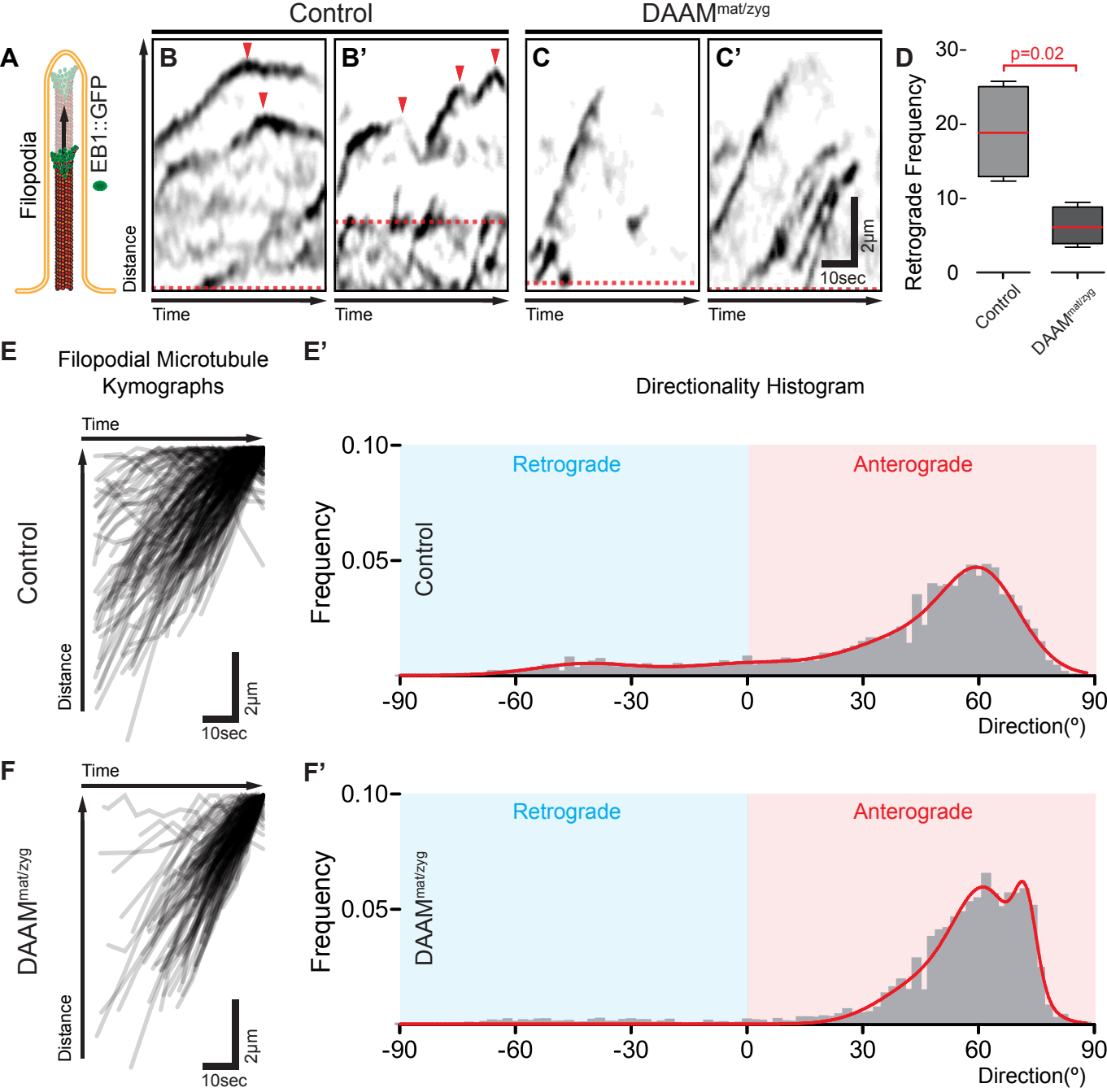
Control
DAAM mat/zyg
A
Filopodia
EB1::GFP
Distance
B
B'
C
C'
Time
2µm
10sec
D
Retrograde Frequency
p=0.02
Control
DAAM mat/zyg
E
Filopodial Microtubule Kymographs
E'
Directionality Histogram
Control
Retrograde
Anterograde
Frequency
Direction(°)
F
F'
DAAM mat/zyg

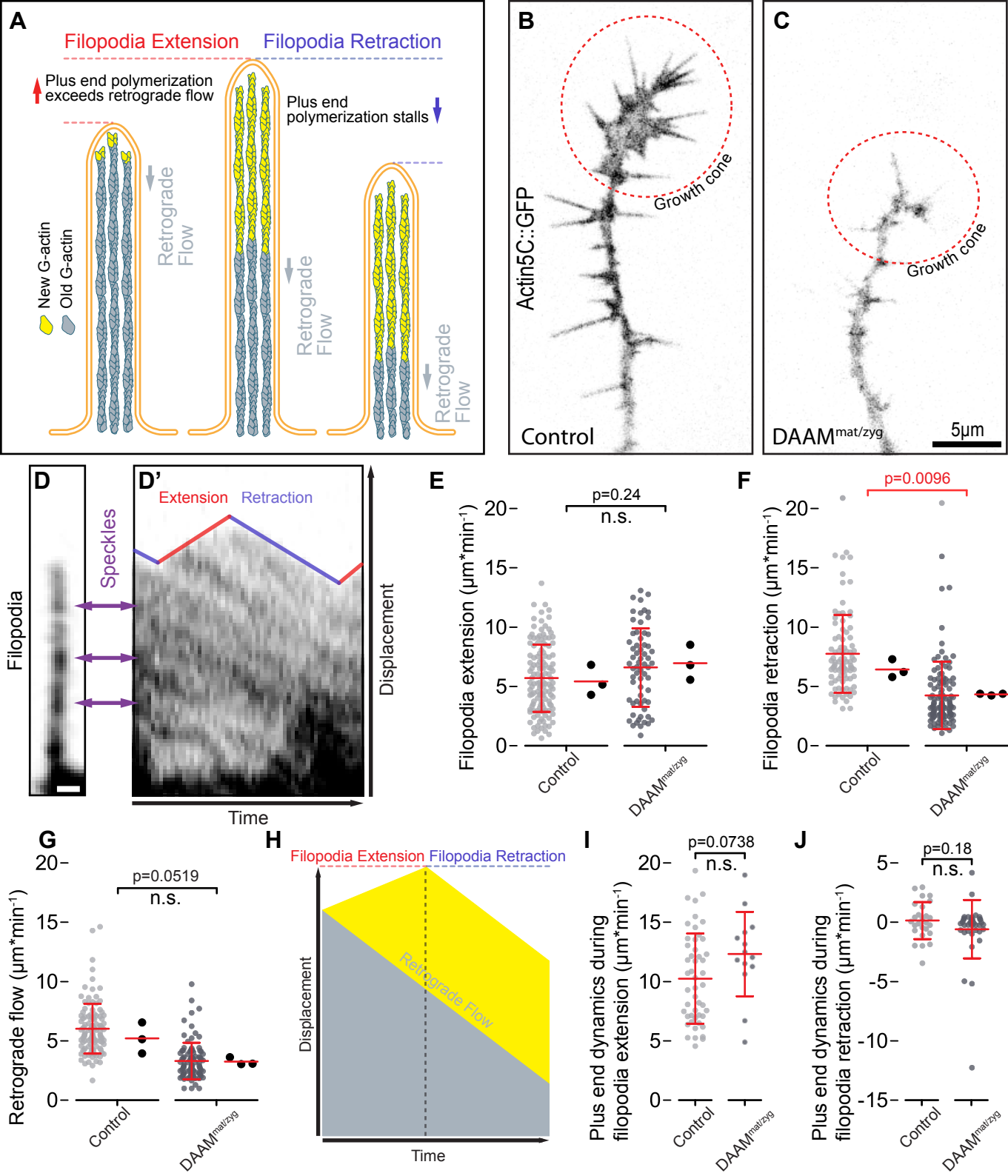
A
Filopodia Extension
Filopodia Retraction
Plus end polymerization exceeds retrograde flow
Plus end polymerization stalls
New G-actin
Old G-actin
Retrograde Flow
Retrograde Flow
Retrograde Flow
B
Actin5C::GFP
Growth cone
Control
C
Growth cone
DAAMmat/zyg
5µm
D
Filopodia
Speckles
D'
Extension
Retraction
Displacement
Time
E
Filopodia extension (µm*min-1)
p=0.24
n.s.
Control
DAAMmat/zyg
F
Filopodia retraction (µm*min-1)
p=0.0096
Control
DAAMmat/zyg
G
Retrograde flow (µm*min-1)
p=0.0519
n.s.
Control
DAAMmat/zyg
H
Filopodia Extension
Filopodia Retraction
Displacement
Retrograde Flow
Time
I
Plus end dynamics during filopodia extension (µm*min-1)
p=0.0738
n.s.
Control
DAAMmat/zyg
J
Plus end dynamics during filopodia retraction (µm*min-1)
p=0.18
n.s.
Control
DAAMmat/zyg

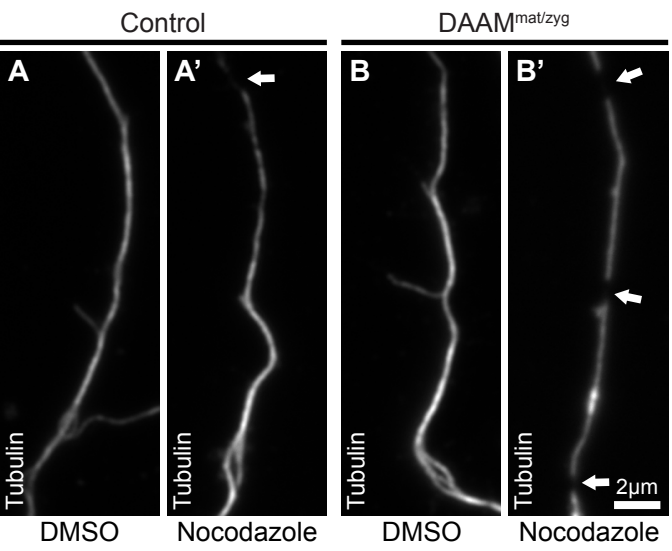
Control
DAAM mat/zyg
A
A'
B
B'
Tubulin
2μm
DMSO
Nocodazole
DMSO
Nocodazole

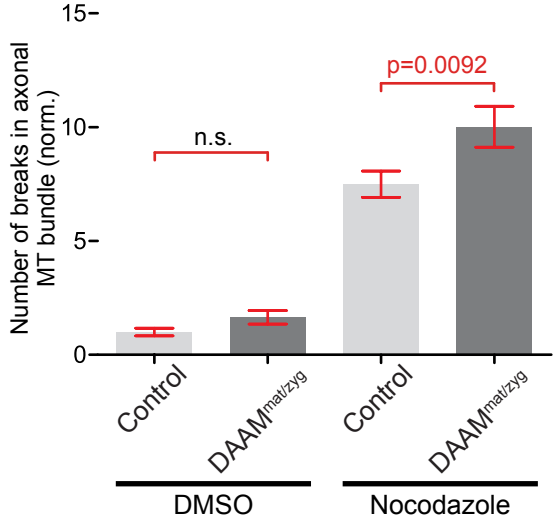
C
Number of breaks in axonal MT bundle (norm.)
15
10
5
0
n.s.
p=0.0092
Control
DAAM mat/zyg
Control
DAAM mat/zyg
DMSO
Nocodazole

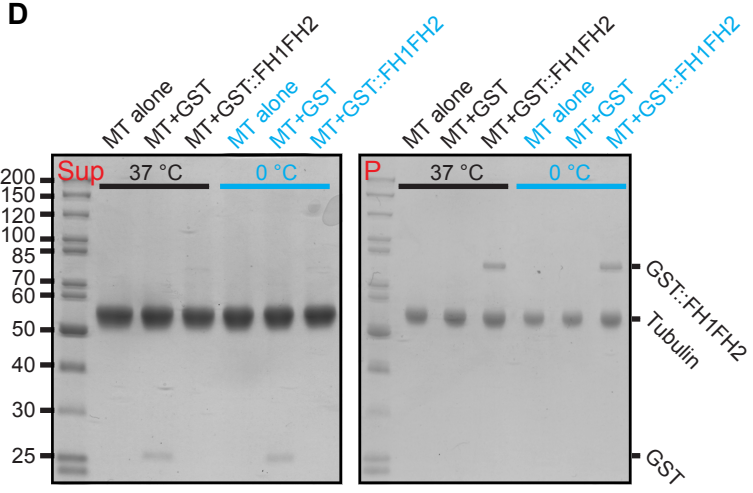
D
MT alone
MT+GST
MT+GST::FH1FH2
MT alone
MT+GST
MT+GST::FH1FH2
Sup
37 °C
0 °C
P
37 °C
0 °C
200
150
120
100
85
70
60
50
40
30
25
GST::FH1FH2
Tubulin
GST

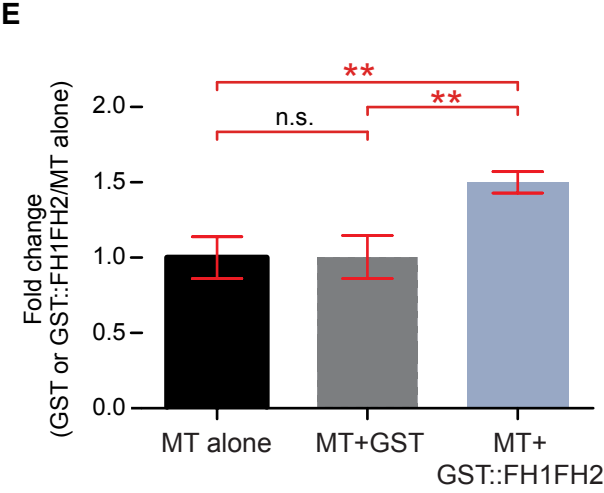
E
Fold change (GST or GST::FH1FH2/MT alone)
2.0
1.5
1.0
0.5
0.0
**
**
n.s.
MT alone
MT+GST
MT+ GST::FH1FH2

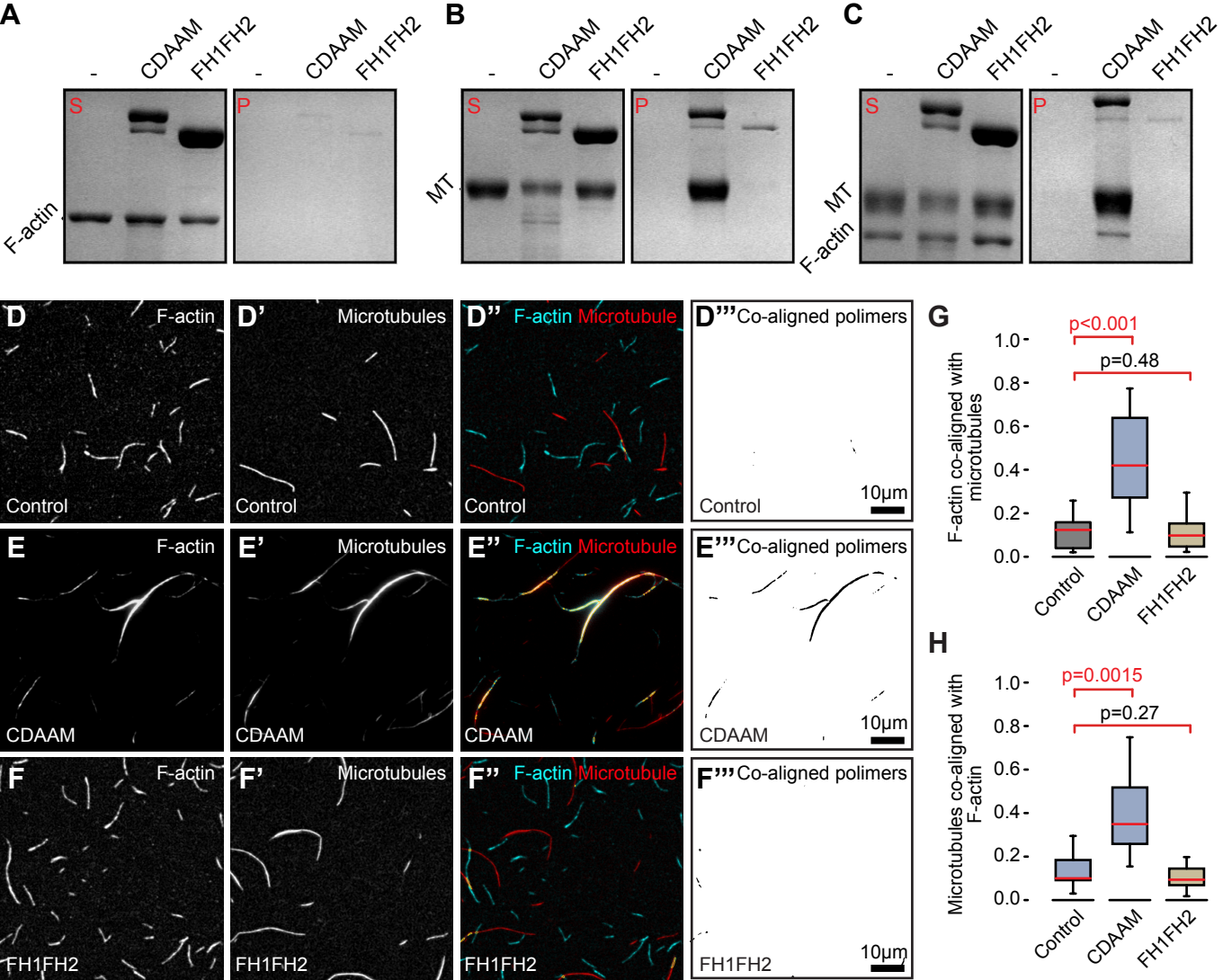
A
B
C
-
CDAAM
FH1FH2
S
P
F-actin
MT
D
F-actin
D'
Microtubules
D''
F-actin Microtubule
D'''Co-aligned polimers
Control
10μm
E
E'
E''
E'''Co-aligned polimers
CDAAM
F
F'
F''
F'''Co-aligned polimers
FH1FH2
G
F-actin co-aligned with microtubules
p<0.001
p=0.48
1.0
0.8
0.6
0.4
0.2
0.0
H
Microtubules co-aligned with F-actin
p=0.0015
p=0.27

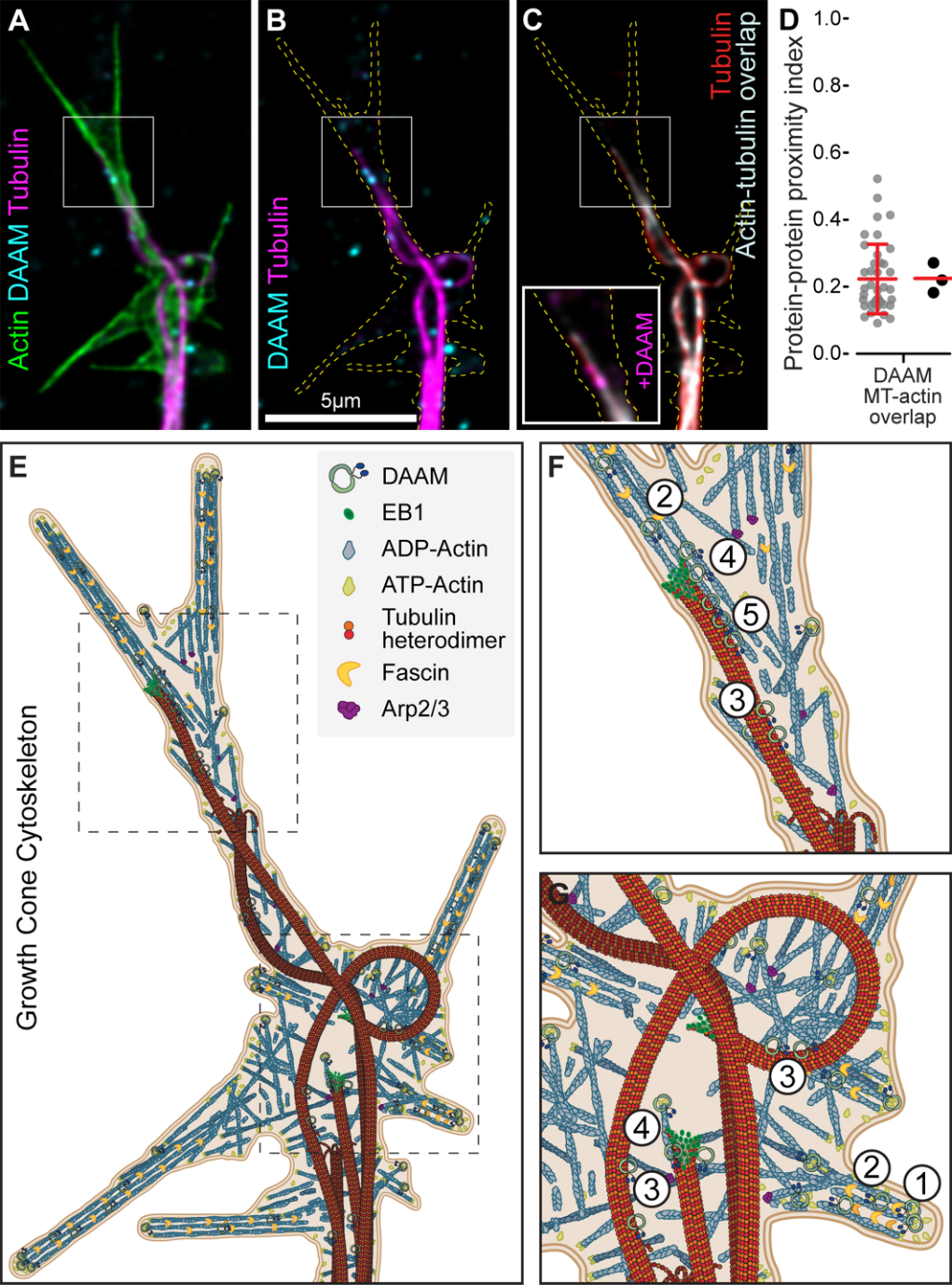
A
Actin DAAM Tubulin
B
DAAM Tubulin
5μm
C
Tubulin
Actin-tubulin overlap
+DAAM
D
Protein-protein proximity index
1.0
0.8
0.6
0.4
0.2
0.0
DAAM MT-actin overlap
E
DAAM
EB1
ADP-Actin
ATP-Actin
Tubulin heterodimer
Fascin
Arp2/3
Growth Cone Cytoskeleton
F
2
4
5
3
G
3
4
3
2
1

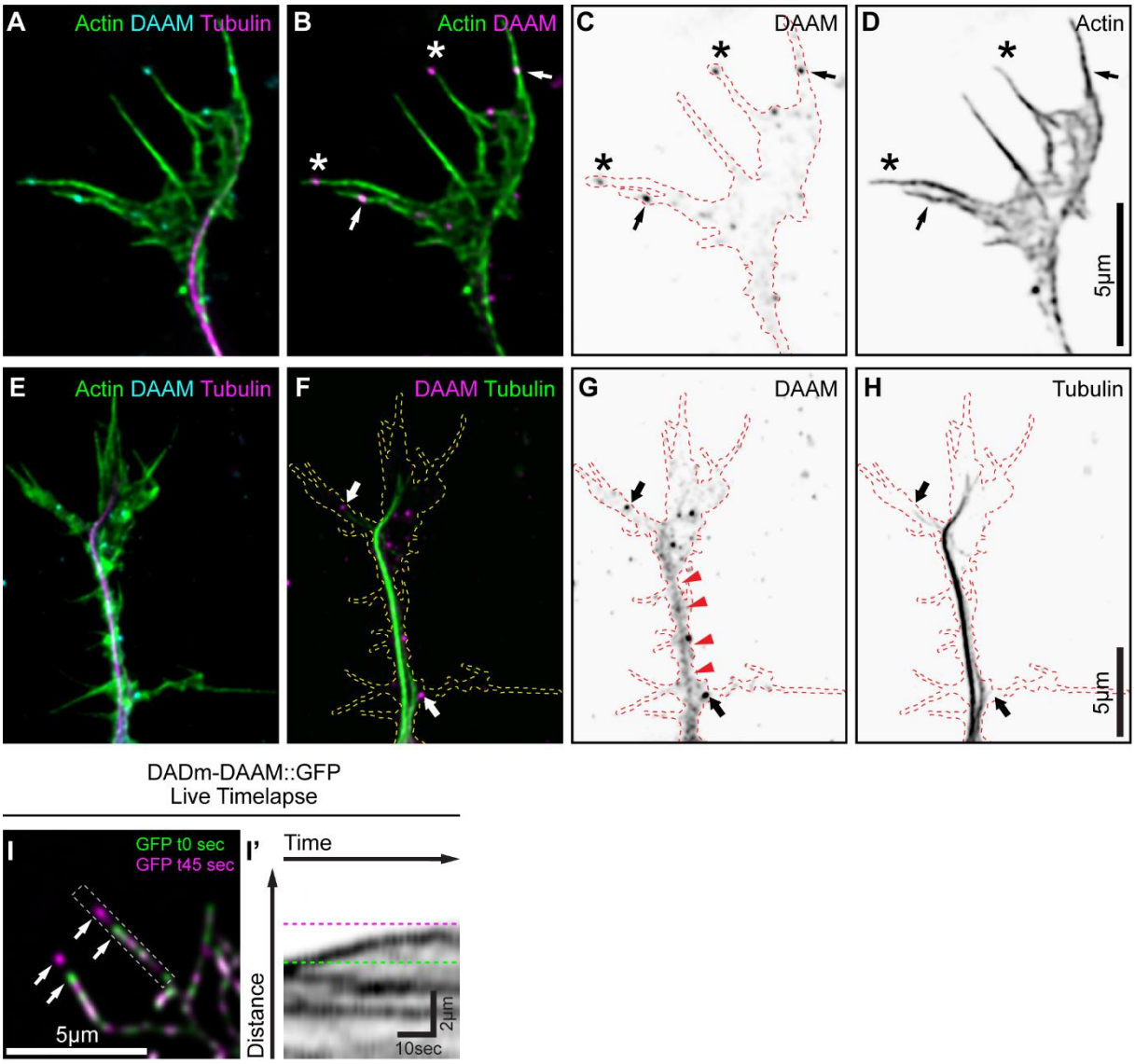

Supplementary Figure 1. Axonal localization of the DAAM protein

(**A-D**) Growth cone of a primary neuron after 6 hours in culture, labeled against F-actin, tubulin and DAAM. Arrows point to DAAM puncta localized along the shaft of filopodia while the asterisks mark the filopodial tip localization. The red dotted line on **C** marks the outline of the growth cone. (**E-H**) Axon of a primary neuron after 6 hours in culture labeled against F-actin, tubulin and DAAM. DAAM localization is detected here with a second, independently created DAAM antibody. Arrows point to DAAM puncta localized at the end of microtubules and arrowheads (red) point to DAAM puncta localized along microtubules. The yellow dotted line marks the outline of the growth cone. (**I, I'**) Images demonstrate the localization and dynamics of DADm-DAAM::GFP. (**I**) Temporal color coded images from a time-lapse sequence capturing filopodia of a neuron expressing DADm-DAAM::GFP. Arrows show that the DADm-DAAM::GFP puncta processively localized to filopodia tip. (**I'**) A kymograph

demonstrating the displacement of DADm-DAAM::GFP along the filopodia marked with white dotted rectangle.

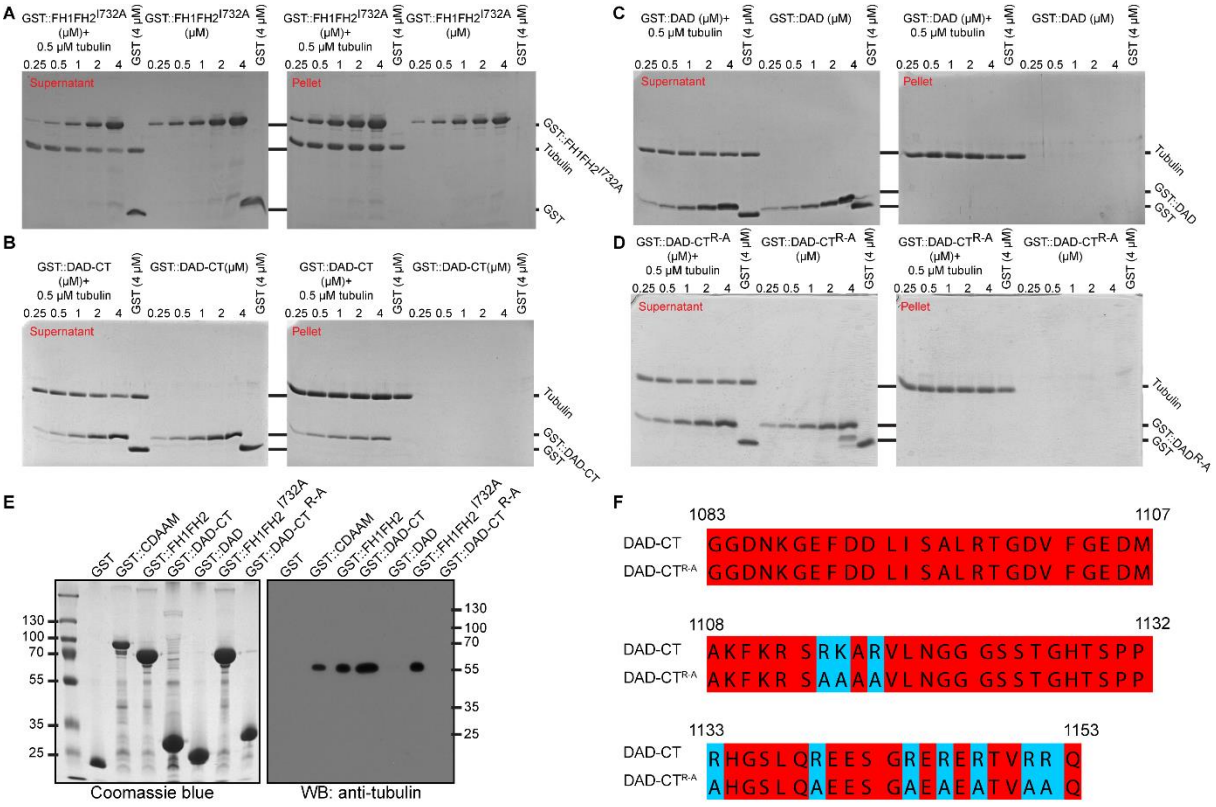

Supplementary Figure 2. The MT binding activity of DAAM by co-sedimentation and GST pull-down assays

(A-D) MT co-sedimentation assays reveal direct physical interaction between MTs and FH1FH2^{I732A} and DAD-CT. Conversely, DAD and DAD-CT^{R-A} do not co-sediment with MTs as they were not detected in the pellets. (**E**) GST pull-down assay shows that MTs physically interact with CDAAM, FH1FH2, FH1FH2^{I732A} and DAD-CT constructs, while MT binding is not observed for DAD and DAD-CT^{R-A}. **(F) Amino acid sequence alignment of DAD-CT and DAD-CT^{R-A} constructs. Letters in blue indicate which basic amino acids (R or K) were mutated to alanines.**

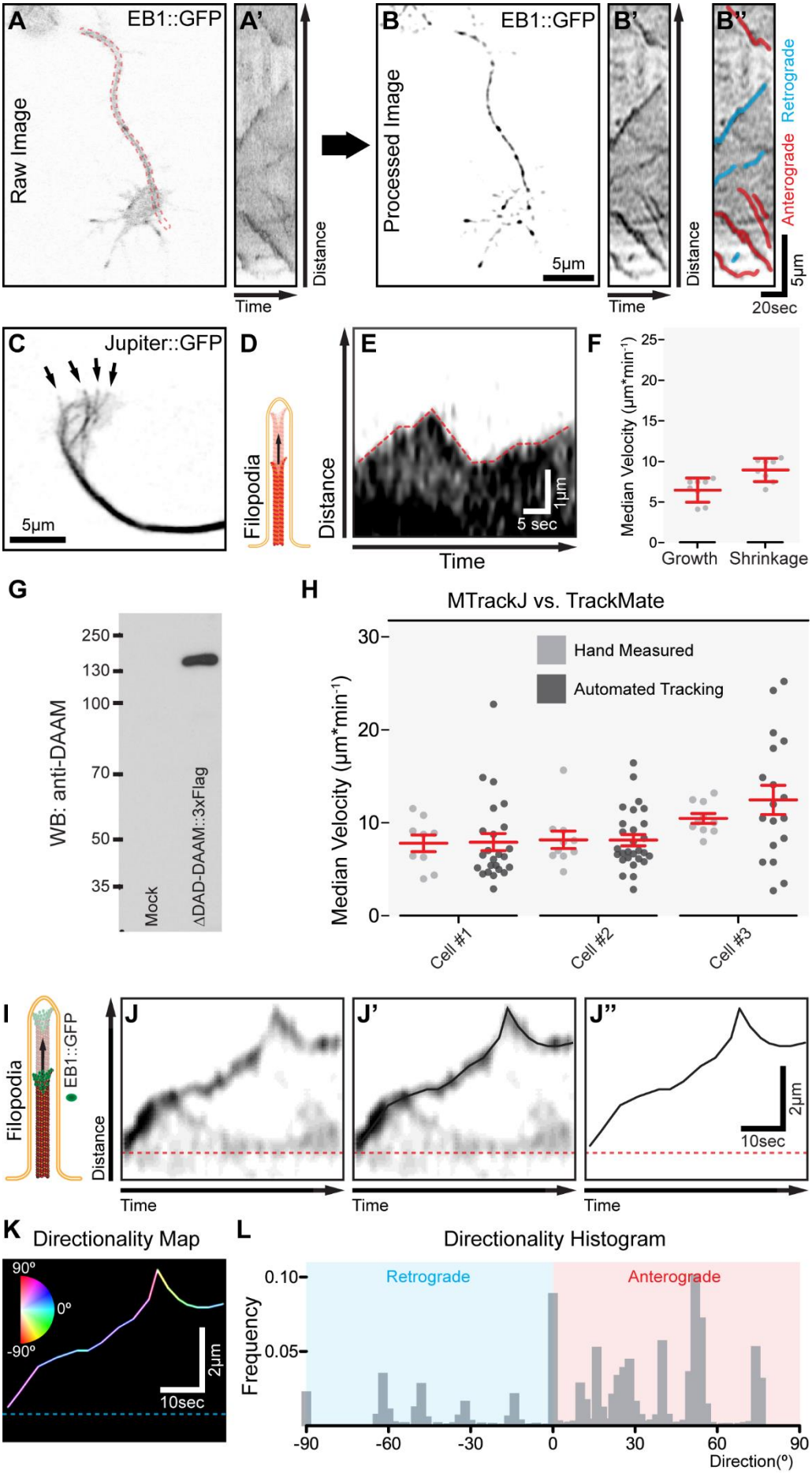
A
EB1::GFP
Raw Image
A'
Distance
Time
B
EB1::GFP
Processed Image
5µm
B'
Distance
Time
B''
Retrograde
Anterograde
5µm
20sec
C
Jupiter::GFP
5µm
D
Filopodia
E
Distance
1µm
5 sec
Time
F
Median Velocity (µm*min-1)
25
20
15
10
5
0
Growth
Shrinkage
G
WB: anti-DAAM
250
130
100
70
50
35
Mock
ΔDAD-DAAM::3xFlag
H
MTrackJ vs. TrackMate
Hand Measured
Automated Tracking
Median Velocity (µm*min-1)
30
20
10
0
Cell #1
Cell #2
Cell #3
I
Filopodia
EB1::GFP
Distance
Time
J
J'
J''
2µm
10sec
K
Directionality Map
90°
0°
-90°
2µm
10sec
L
Directionality Histogram
Retrograde
Anterograde
Frequency
0.10
0.05
-90
-60
-30
0
30
60
90
Direction(°)

Supplementary Figure 3. Measuring microtubule dynamics and retrograde translocation

(**A**) Still image from a time-lapse sequence showing EB1::GFP comets in a primary neuron. (**A'**) A kymograph recorded along the neurite (red dotted area) reveals microtubule growth. (**B**) EB1::GFP recordings were deconvolved with a small S/N ratio to remove background and to enhance signal. Following that, the EB1::GFP signal was further enhanced by a custom made Difference of Gaussian filter. (**B', B''**) Kymographs recorded in the processed sequences demonstrated signal enhancement and improved tracking of microtubule growth. (**C**) Neurite of a primary neuron expressing Jupiter::GFP. Arrows point to microtubule ends in the growth cone. (**D**) The drawing illustrates a growth cone filopodia invaded by a microtubule. (**E**) Microtubule dynamics in Jupiter::GFP expressing neurons can be measured by kymographs recorded along the growth cone filopodia. (**F**) Scatter plots show microtubule growth and shrinkage velocity measured in Jupiter::GFP expressing neurons. Grey dots represent the median values measured on individual cells with median and interquartile range. **(G) Validation of the specificity of the newly generated DAAM antibody (#4938). Anti-DAAM (#4938) detected the ΔDAD-DAAM::3xFlag protein specifically from an S2 cell lysate, whereas no signal was observed in control samples.** (**H**) Scatter plots show comparison of individual microtubule velocities measured by hand (MTrackJ) or by semi-automatically (TrackMate). (**I**) The cartoon illustrates a growth cone filopodia invaded by a microtubule where the growing plus-end is labeled with EB1::GFP. (**J-J''**) EB1::GFP kymographs were recorded along growth cone filopodia using KymoResliceWide, a Fiji plugin dedicated to generate kymographs with improved contrast. The centerline of these kymographs were manually extracted as binary images. (**K, L**) Using the local gradient orientation method the directionality plugin of Fiji computes a directionality map (**K**) and a histogram (**L**), indicating the amount of structures in a given direction. In these directionality histograms negative values represent the retrograde translocation, zero represent pause and positive values represent anterograde movement. Histograms give a peak at the preferred orientation which is proportionate to the preferred velocity of the EB1::GFP spots.

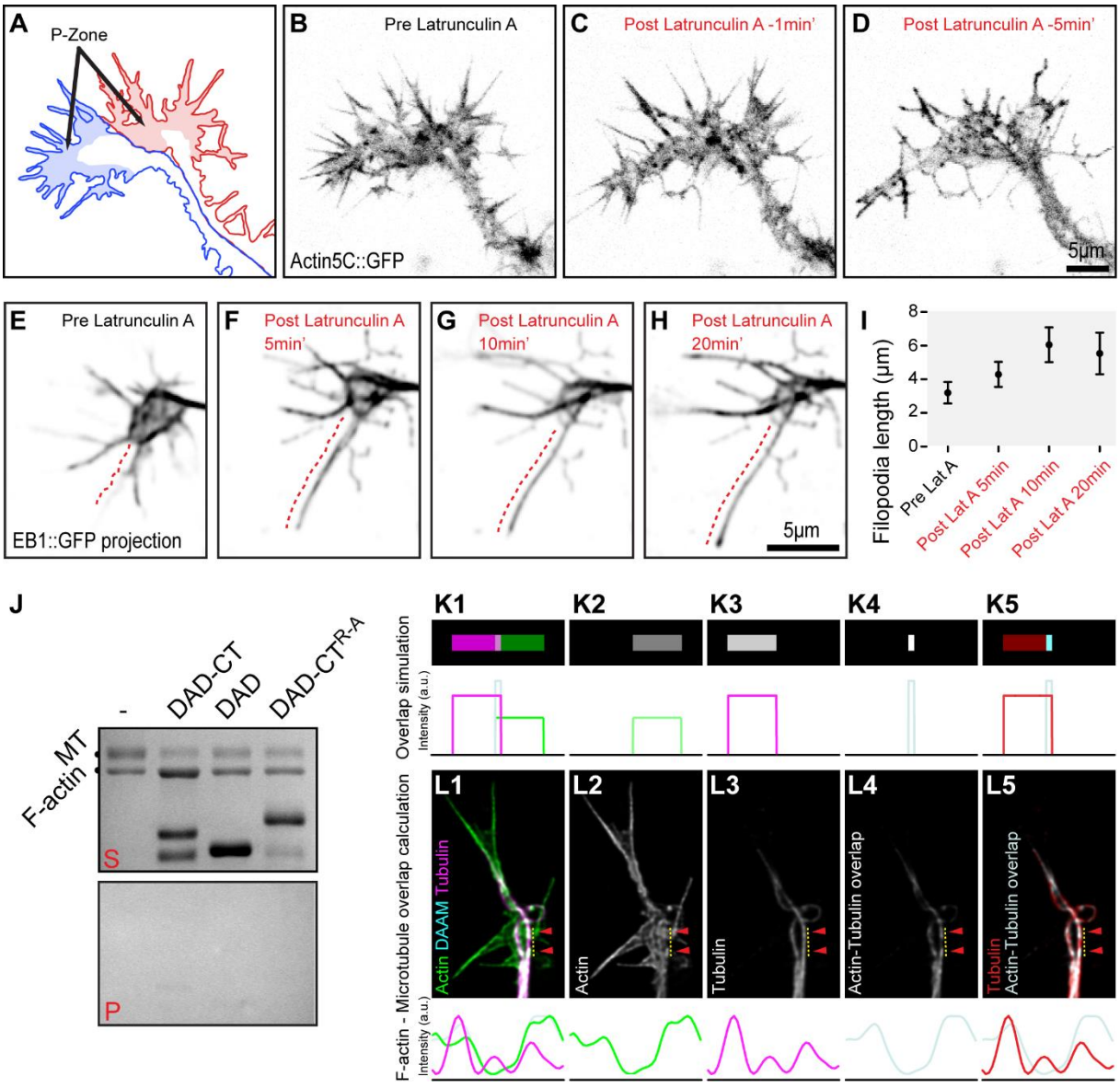

Supplementary Figure 4. Effect of latrunculin A on cytoskeleton dynamics, and an F-actin – microtubule overlap analysis

(**A**) Schematic illustration of the peripheral zone of two neurites shown on panels B-D. (**B-D**) Effect of latrunculin A (200 nM) on the actin cytoskeleton of neurons expressing Actin5C::GFP. (**E-H**) Effect of latrunculin A (200 nM) on microtubule dynamics of neurons expressing EB1::GFP. (**I**) Graph shows the effect of latrunculin A (200 nM) on the length of filopodia like protrusions. (**J**) Representative Coomassie-stained SDS-PAGE gel from low-speed centrifugation experiment through a sucrose gradient showing the amount of microtubules (MT) and F-actin (FA) in the supernatants (S) and in the pellets (P) in the absence or presence of either DAD-CT, DAD or DAD-CT^{R-A}, as indicated. The lack of MTs and F-actin in the pellet indicates that these regions of DAAM neither bundle nor co-align these polymers.

(**K1-5**) Simulation demonstrates that multiplication of images (K2 and K3) with partially overlapping structures (K1) with zero background will result in an image where only the overlapping structure is visible (K4, K5). (**L1-5**) The same principles were applied to biological images to generate the 'overlap signal' which was used to quantify the DAAM fraction localized to the overlapping F-actin and microtubule regions. We multiplied the F-actin (L2) and microtubule (L3) images to recover the overlapping areas visible in L1. In biological images, the relatively high background generates artifacts, therefore, we deconvolved our images to reduce the background to a negligible level. As a result, the following multiplication represents the overlapping filaments faithfully and excludes all the non-overlapping voxels (L4 and L5). Using floating 32-bit file format allows scaling of the results, thereby preventing clipping of the overlap signal.

Movie 1. Filopodial localization and dynamics of DADm-DAAM::GFP.

Movie 2. Microtubule growth analysis.

MT dynamics were analyzed from EB1::GFP time lapse recordings, using TrackMate. The EB1::GFP recordings were deconvolved with a small S/N ratio to remove background and to enhance signal. Following that, the EB1::GFP signal was further enhanced by a custom made Difference of Gaussian filter. After that, EB1::GFP tracks were analyzed separately. To reduce the ratio of false trajectories all the tracks that could not be followed for at least four consecutive frames were discarded. For the spot detection, we used the LoG detector and the simple LAP tracker were used to link the spots. Gap closing was allowed for one frame gaps.

Movie 3. Microtubule growth velocity visualized by EB1::GFP in control and *DAAM*$^{mat/zyg}$ mutant neurons.

Movie 4. Effect of latrunculin A (200 nM) on the actin cytoskeleton of neurons expressing Actin5C::GFP.

Actin cytoskeleton starts to breakdown as early as 30-60 seconds after treatment and the stereotypic searching movements of filopodia completely disappear after ~5 minutes.

Movie 5. Effect of latrunculin A (200 nM) on microtubule dynamics and on the length of filopodia like protrusions in primary neurons expressing EB1::GFP.

Movie 6. Filopodia and actin dynamics (extension, retraction, actin polymerization and retrograde flow) of a primary neuron (6 HIV) expressing Actin5C::GFP.

Primer name	Sequence	Purpose
dDAAM-732A-F	CACCGCTCTGCTGAGCAAACTG	I732A mutant
dDAAM-732A-R	CAGTTCTGCGCCCGACGTCC	I732A mutant
DAD 1F	GGAATTCATGGCGGCGACAACAAGGGCGAG	DAD and DAD-CT fragment
DAD 1R	GGAATTCACGCGCGCCTTGCGCGACCGCTT	DAD fragment
CDAAM-1R	GGAATTCTGGCGCCTCACGGTCCGCTC	DAD-CT fragment
DAD 5' R	CTTTGCCGGGGAGTCAGGATC	ΔDAD-DAAM
DAD 3' F	CTTAACGGCGGCGGATCCTC	ΔDAD-DAAM
DAD-CT^{RA} oligo	ATGGAGCTCAAAAAGCGCACAATAGAGCGCAAGAACAAG ACCGGCCTAATGACCAGCGTGGCTCGCAATCTGGGCCTCAA GTCAGGCTCTTCCAACGGGGATCCTGACTCCCCGGCAAAGG GCGGCGACAACAAGGGCGAGTTTGACGATCTCATCTCGGC CCTGAGGACCGGCGACGTGTTTGGCGAGGACATGGCCAAG TTCAAGCGGTCGGCCGCGGCGGCCGTGCTTAACGGCGGCG GATCCTCCACTGGGCACACCTCGCCGCCCGCCCACGGCAGC CTCCAAGCGGAGGAGAGTGGGGCTGAGGCCGAGGCGACC GTGGCGGCCCAGAATTCGGCGCCGCACTCGGCATATCTAGA GCT	DAD-CT^{R-A} fragment

Table 1. List of primer sequences used in this study.